

TISSUE ENGINEERED BONE MODELS: ADVANCES IN 3D PRINTED TRICALCIUM
PHOSPHATE/POLYLACTIDE (TCP/PL) SCAFFOLDS

by

BRETT RITCHEY

(Under the Direction of Dr. Karen Burg)

ABSTRACT

Metastasis to bone occurs in approximately 70% of patients with advanced breast cancer, and in most cases treatment will not be successful. In 2024, it is expected that within the U.S. alone there will be 313,510 new cases of breast cancer resulting in 42,780 deaths. Current understanding of the specific biological mechanisms of bone metastasis is incomplete. Two-dimensional *in vitro* models of bone cancer are too simple to elucidate these mechanisms while *in vivo* models may be too complex to study specific protein roles or cell-cell interactions. This work focuses on the development and characterization of a tissue engineered 3D model of human bone. It is hoped that by using a commercially available 3D printer, this work will provide a process for developing effective models of the human bone niche that will be used to increase our understanding of breast cancer metastasis to bone and inform the development of improved treatments.

INDEX WORDS: bone, metastasis, models, scaffolds, 3D-printing, tissue engineering

TISSUE ENGINEERED BONE MODELS: ADVANCES IN 3D PRINTED TRICALCIUM
PHOSPHATE/POLYLACTIDE (TCP/PL) SCAFFOLDS

by

Brett Ritchey

BS, University of Georgia, 2022

A Thesis Submitted to the Graduate Faculty of The University of Georgia in Partial Fulfillment
of the Requirements for the Degree

MASTER OF SCIENCE

ATHENS, GEORGIA

2024

© 2024

Brett Ritchey

All Rights Reserved

TISSUE ENGINEERED BONE MODELS: ADVANCES IN 3D PRINTED TRICALCIUM
PHOSPHATE/POLYLACTICE (TCP/PL) SCAFFOLDS

by

Brett Ritchey

Major Professor:	Karen Burg
Committee:	Timothy Burg
	Cheryl Gomillion

Electronic Version ApDemonstrated:

Ron Walcott
Vice Provost for Graduate Education and Dean of the Graduate School
The University of Georgia
May 2024

DEDICATION

I dedicate this page to all the students, teachers, family, and friends I have met both during and before my time at UGA that have contributed to my academic career and encouraged me to nurture my desire to learn.

ACKNOWLEDGEMENTS

I offer special thanks to my major professor, Dr. Karen Burg, and my advisory committee consisting of Dr. Timothy Burg and Dr. Cheryl Gomillion. I acknowledge Dr. Weitong Chen and my fellow students in the Harbor Lights Laboratory who have assisted my efforts on this project.

I am thankful to the faculty and mentors I have had at UGA that have taught me the skills I used on this project, and for the peers that aided me while I was learning them. I am also very grateful to my family for their support while working towards my degree.

TABLE OF CONTENTS

	Page
ACKNOWLEDGEMENTS	v
LIST OF TABLES	viii
LIST OF FIGURES	ix
CHAPTER	
1 INTRODUCTION AND LITERATURE REVIEW	1
Background	1
Bone Structure and Function	2
Scaffold Requirements for Bone Tissue Modelling.....	3
Synthesis of Research Opportunity from Key Findings in Literature	7
Hypothesis, Research Questions, and Objectives	12
Significance of the Study	13
2 COMPOSITE CHARACTERIZATION AND SCAFFOLD PRODUCTION.....	14
Composite Material Preparation	15
Thermal Characterization.....	16
Filament Extrusion.....	23
Scaffold Design and 3D Printing	27

	Mechanical Testing.....	38
3	CELL/SCAFFOLD INTERACTIONS.....	45
	Cell Adhesion Experiments with MC3T3 Cells	45
	Cell Viability and Proliferation with MC3T3 Cells.....	50
4	DISCUSSION AND CONCLUSIONS	54
	Summary of Key Findings	54
	Interpretation of Results.....	54
	Limitations and Future Directions	56
	Conclusion	56
5	REFERENCES	58
6	APPENDIX A: FLOWCHART.....	63

LIST OF TABLES

	Page
Table 2.1: ANOVA statistics for fourth cycle DSC data for pure PL, 55% TCP by mass composite as prepared, and 55% TCP by mass composite after filament extrusion and 3D printing.....	21
Table 2.2: ANOVA statistics for diameter analysis of 55% TCP composite filament composite extruded at 165°C.....	26
Table 2.3: Summary statistics for diameter analysis of 55% TCP composite scaffolds.....	37
Table 2.4: Welch's t-test for scaffold diameter of 55% TCP composite filament composite extruded at 165°C.....	38
Table 3.1: Statistics for cell adhesion of MC3T3 cells onto porous scaffolds made of pure PL..	49

LIST OF FIGURES

	Page
Figure 1.1: Left - Healthy Trabecular Bone with a sawn surface. Right - Osteoporotic bone (non-sawn).....	3
Figure 1.2: Scope of the project outlining how a COTS printer could potentially be used to produce a tissue test system	8
Figure 1.3: Diagram of a typical 3D printer head detailing components and motion that could create a scaffold.	11
Figure 2.1: Photos of the material preparation process.....	16
Figure 2.2: Left - As received PL pellets. Right - PL fiber after extrusion.	17
Figure 2.3: DSC thermogram of a 6mg sample of pure PL.....	20
Figure 2.4: DSC thermogram of a 10mg sample of 55% TCP/PL composite as prepared.....	20
Figure 2.5: DSC thermogram of 10mg sample of printed 55% TCP/PL composite.	21
Figure 2.6: An extruded filament being measured; units are in centimeters.	26
Figure 2.7: Right-Top view showing the first two strut layers of a lattice structure showing struts were spaced 400µm apart.	28
Figure 2.8: Composite lattice structure printed with a PrusaMK3S.	29
Figure 2.9: Top Left- Healthy trabecular bone. Bottom Left- Osteoporotic bone with trabecular distance. Top Center- Two strut levels of the square lattice in PrusaSlicer. Bottom Center- bottom layer of the gyroid geometry produced with 50% infill setting in PrusaSlicer. Top Right-	

bottom layer of the gyroid geometry produced with 60% infill setting in PrusaSlicer. Bottom Right- bottom layer of a hexagonal 60% infill pattern. 30

Figure 2.10: Top Left- PL scaffold produced with 70% gyroid infill. Bottom Left- PL scaffold produced with 60% hexagonal and black filament. Top Right- PL scaffold produced with 60% infill. Bottom Right- PL scaffold produced with 50% gyroid infill. 32

Figure 2.11: Top view of a 50% gyroid infill model in the PrusaSlicer software showing pore structure..... 33

Figure 2.12: Image of a 60% gyroid infill model in the PrusaSlicer software showing pore structure with intended pore diameter..... 34

Figure 2.13: Oblique top and side perspective of a sliced scaffold; the sides are porous as well. 34

Figure 2.14: Top view of a composite scaffold produced with 60% infill setting with scale bar, taken by stereoscope. 35

Figure 2.15: Top view of a composite scaffold produced with 50% infill showing pore structure with scale bar, taken by stereoscope. 36

Figure 2.16: Graph of a 55% TCP compression sample..... 40

Figure 2.17: Stereoscopic image of the compression surface of a composite sample. 42

Figure 2.18: The interior portion of a compression sample..... 42

Figure 2.19. Comparison of effective E for samples of pure PL and 55% TCP/PL compression samples..... 43

Figure 3.1: Adhesion study results showing the number of cells adhered to the scaffolds. 48

Figure 3.2: Percent alamarBlue™ normalized around averages of the control. Scaling factor for standard deviation was 0.05..... 52

CHAPTER 1

INTRODUCTION AND LITERATURE REVIEW

Background

According to statistics reported yearly by the American Cancer Society, in 2024 it is estimated that within the U.S. alone there will be 313,510 new cases of breast cancer resulting in 42,780 deaths¹. Cancer that spreads from a starting point to other parts of the body is called metastatic cancer (labeled "stage IV" for many cancer types), the process of spreading is called metastasis². In cases of advanced breast cancer, metastasis to bone occurs in approximately 70% of patients^{3,4}. Recent studies suggest that the bone environment may serve as a "transfer station" for further distribution of breast cancer⁵. Treatments for bone metastasis are often complex, involving multidisciplinary teams of radiologists, oncologists, and orthopedic surgeons⁶ yet rarely are any of these treatments fully successful⁴. It is thought that a better understanding of the underlying molecular pathways in bone metastasis could lead to more successful treatments⁷; however, the medical and scientific community's current understanding of the specific biological mechanisms involved in bone metastasis remains incomplete⁸.

In 1989, Paget's "Seed and Soil" theory presented the hypothesis that cancer metastasis is based on a characteristic selection of organs (the soil) by cancer cells (the seed)⁹. Since then, extensive research has not only provided evidence in support of this theory but has also partially revealed the specific mechanisms behind metastasis¹⁰. Two-dimensional *in vitro* models of bone cancer are often too simple to reveal these mechanisms, while *in vivo* models are often too complex to allow feasible study of specific protein roles or cell-cell interactions¹¹. This work

focuses on the development, refinement, and characterization of a tissue-engineered *in vitro* 3D model of human bone that will create an option that allows a sufficiently complex, tunable, repeatably constructed system. With the ability to use a commercial off the shelf (COTS) 3D Fused Deposition Modeling (FDM) printer to create on demand models of human bone, clinicians and researchers would be able to readily build tissue test systems that can be more easily and accurately studied.

Bone Structure and Function

Bone is a highly complex mineralized connective tissue that supports four types of cells: osteoblasts, osteoclasts, osteocytes, and bone lining cells¹². The dynamic nature of bone is such that it is continuously resorbed by osteoclasts and reformed by osteoblasts. The hierarchal structure of bone can be separated into a dense outer layer called cortical (compact) bone which provides protection and mechanical strength, and an inner layer called trabecular (cancellous/spongy) bone that contains a large porous matrix that supports cell growth¹³.

Trabecular bone has been found to be the preferred site for breast cancer metastasis following hematogenous spread¹⁴; therefore, it should be the primary type of bone modeled for cancer studies. Osteoporosis, a bone disorder categorized by a loss of bone tissue, is a well-documented condition following metastasis and subsequent treatment. Figure 1.1 contains examples of normal and osteoporotic bone, the images suggest that the osteoporotic bone matrix is thinner and that there is more open void space.

The pore size (diameter) of samples of healthy trabecular bone sourced from the human femoral head, dried and analyzed using mercury intrusion porosimetry, were found to have a pore diameter in a range of 5 - 950 μm ¹⁵. The pore size of thirty-five samples of osteoporotic bone taken from human femoral heads were studied with low-field magnetic resonance (LF-

NMR) and microcomputed tomography (micro-CT), finding the distribution of pore size in the largest class of osteoporotic bone to have a mean and standard deviation of $623 \pm 415\mu\text{m}$ ¹⁶.

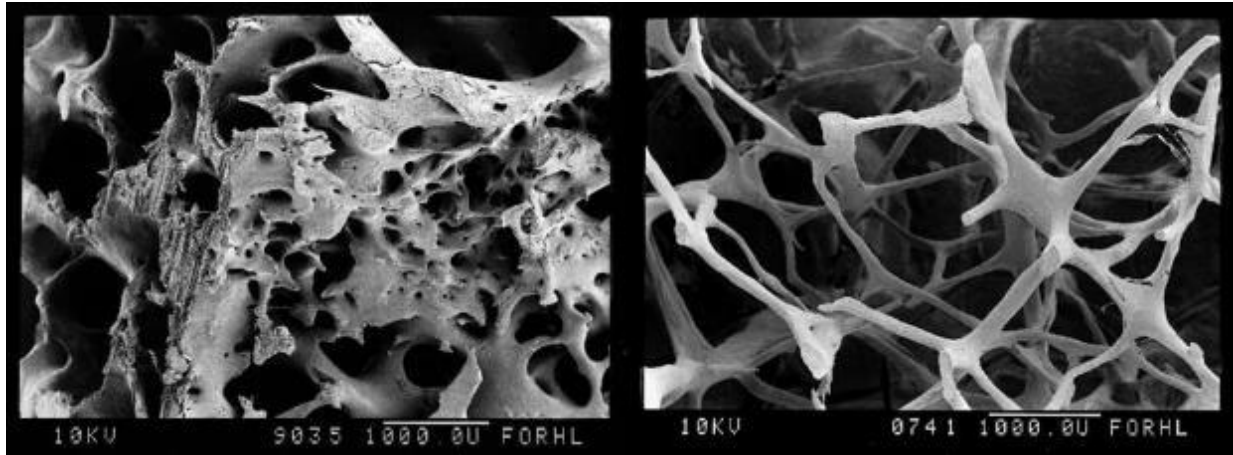


Figure 1.1: Left - Healthy Trabecular Bone with a sawn surface. Right - Osteoporotic bone (non-sawn). (Credit: SEM bone, sawn surface + fracture face. SEM old osteoporotic bone. David Gregory & Debbie Marshall. Attribution 4.0 International (CC BY 4.0). Source: Wellcome Collection. Accessed 4/3/2023 at <https://wellcomecollection.org>).

Scaffold Requirements for Bone Tissue Modelling

In tissue engineered models of bone, 3D scaffolds are used to represent mineralized connective tissue. As with any model, the expected use of the model will define the required fidelity over a specific range of conditions. Given the complexity of the bone niche, it is unrealistic to expect that any model could recapitulate all the properties of the native bone. A model, by definition, has limitations and approximations. The scaffolds could thus be tailored to needs specific to a model for a particular biological question or disease process. For example, a scaffold may need an extracellular matrix (ECM) that supports bone cell attachment and proliferation¹⁷.

When designing tissue engineered scaffolds intended to model specific aspects of human bone, considerations at various structural levels must be considered. Macrostructural elements, such as overall shape and dimensions, impact the mechanical stability of the scaffold and the type of testing/seeding methods that can be used on the scaffold. Microstructural features such as pore size, geometry, and the interconnectivity of pores influence cell adhesion and proliferation and may be the focus of a specific project dictating scaffold requirements. Macrostructural features influence cell migration, cell proliferation, and mineralization, which contribute to new bone tissue formation. Additionally, the nanoscale surface properties of the scaffold, such as hydrophobicity, play a role in cellular adhesion¹⁸ and could be incorporated into models where these factors are dominant, compared to microstructural or macrostructural elements.

Recent Advancements in Tissue Engineered Bone Scaffolds

Scaffolds must possess the right set of properties that contribute to their effectiveness in a specific modeling goal. Materials used in 3D scaffold fabrication significantly influence their performance with hybrid biomaterials being studied in recent years as a promising new avenue¹⁹. Absorbable polymers, such as polylactide (PL), are broken down by the body's natural processes. In the case of PL, the material is eventually reduced into either lactic acid or carbon dioxide and water by hydrolytic reactions. PL has also been used in commercial 3D printers to produce scaffolds viable for MC3T3-E1 (mouse pre-osteoblast) cell studies²⁰. For *in vivo* studies, biocompatibility is important to assess as all implanted materials cause adverse reactions but material choice can determine the response's severity. Bioactive ceramics, like tricalcium phosphate, enhance osteoconduction and provide a mineralized environment conducive to bone formation²¹. Composite materials used in bone tissue engineering often combine polymers and

ceramics with the intention of creating more easily workable materials that have the benefits of solid ceramics, such TCP/PL.

A 2006 study conducted by Aunoble and coworkers²² showed that PL can be used successfully with 60% by mass TCP to produce injection molded implants. After 27 days *in vitro*, the 60% TCP by mass implants facilitated a 120% higher number of human osteogenous cells than on the 30% material, and 220% higher than PL alone. After 6 months of implantation in rabbit femurs, the 60% TCP by mass implants were determined to have similar biological performance to pure TCP implants based on the results of Giemsa staining. It should be noted, however, that while these implants were porous, they possessed a reported pore diameter range of 5-400 μm .

Studies conducted since 2006 have also shown further positive results in the development of ceramic/polymer composites for producing 3D cell scaffolds. Hydroxyapatite has been incorporated in polylactide filaments for 3D printing²³. Pores from 200 to 450 μm with acute and obtuse angles were accurately produced. Hexagonal pores of 450 μm with obtuse angles displayed enhanced mineralization over acute pores and the presence of hydroxyapatite stimulated mineralization and matrix deposition.

For the purposes of bone tissue engineering, most studies recommend curved pore with diameters above 300 μm , citing studies where scaffolds with pores of 500 or 600 μm showed higher osteoconductive potential than scaffolds with larger or smaller pores^{24,25}. More recent studies using advanced computational methods have found similar results^{26,27}. Recommended geometry seems to hold across scaffolds fabricated with different materials as well. In one study²⁸, rat bone marrow-derived mesenchymal stem cells (rBMMSCs) were seeded on porous titanium scaffolds fabricated by vacuum diffusion bonding of titanium meshes. More cell

proliferation and bone ingrowth were seen on the Ti 313 and Ti 390 (313 & 390µm pore size), though the Ti 313 & Ti 390 had their highest respective numbers on different days, with Ti 390 having the highest on day 21 and Ti313 having a lower cell count. Another study conducted on titanium scaffolds found that among two different pore sizes (500µm and 1000µm) and three different pore shapes (triangular, hexagonal and rectangular) the more obtuse angled hexagonal pores of 500µm facilitated the highest amount of human periosteum-derived cells (hPDC)²⁹.

Scaffolds 3D-printed using polycaprolactone (PCL) filament showed less cell proliferation than scaffolds produced with a β -TCP/PCL composite. For chemical compositions of 0% and 20% β -TCP, no significant ($p \leq 0.05$) increase was shown over time, while 40% and 60% ratios indicated a significant increase of activity at day 11 compared to day 1 and 7, with respective increases of 5% and 10%³⁰.

Composites comprising β -TCP/PL have been successfully melt-compounded in a mixing chamber at weight percentages of up to 25% TCP³¹. Differential scanning calorimetry (DSC) and thermogravimetric (TG) analyses were used to evaluate the thermal characteristics of β -TCP/PL samples. While it was found that the melting and glass transition temperatures did not change as TCP mass percentage increased, the temperature at which the initial thermal degradation of the material begins (T_{onset}) was found to lower slightly as TCP content increased. For this reason, the authors speculated that at higher mass percentages, TCP may influence thermodegradation reactions, possibly by inducing hydrolytic cleavage of PL chains during thermal processing. Earlier studies have run similar tests on β -TCP/PL composites of up to 40% TCP³² by mass, drawing similar conclusions based on TGA, but contradicting results from DSC; the glass transition temperature (T_G) was lower in composites that were 10% TCP by mass or higher in the earlier study.

The more recent study by Backes and colleagues³¹ also found that the compressive modulus (E) of the 5% mass TCP and 10% mass TCP composite samples manufactured by hot press increased by 5.2% and 5.8% respectively. At 10% m/m TCP, however, the compressive strength of samples were similar to pure PL. It was speculated that this change in mechanical properties could be due to degradation of the polymer influenced by the addition of TCP. These results contradict an earlier study conducted by Ferri and colleagues³², in which the Young's Modulus increase in samples of up to 30% TCP by mass. In any case, Backes and colleagues³¹ used only the 10% and 5% TCP composites to extrude filament. Twin-screw extrusion was used to produce filaments at 10% TCP with diameters of 1.75 ± 0.03 mm. These filaments were then used in a Sethi S3 FFF 3D printer, successfully producing a set of screws.

(PCL)/(nHA)/CNW nanocomposite fused deposition modeling (FDM) filaments have been manufactured and 3D printed. Using nine experiments recommended by a Taguchi orthogonal array it was found that nozzle temperature had the most significant impact on structural integrity and compressive strength with statistical P-values lower than 0.04 for both³³.

Synthesis of Research Opportunity from Key Findings in Literature

Analysis of the reviewed literature suggests the opportunity, sketched in Figure 1.2, to create new scaffolds for use in tissue test systems through the appropriate print design and modification of a printable filament in a commercial, off-the-shelf (COTS) 3D Fused printing system.

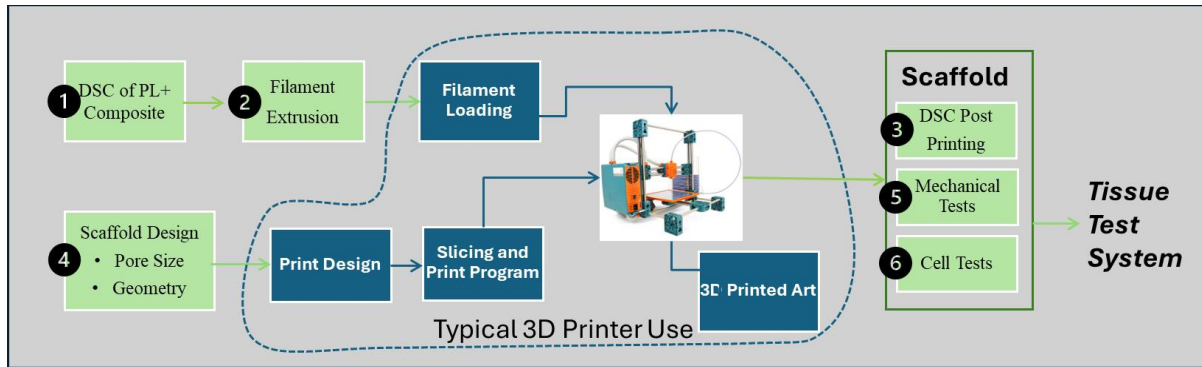


Figure 1.2: Scope of the project outlining how a COTS printer could potentially be used to produce a tissue test system. Credit for the image of the 3D printer in the center: "Sintermask - fabbster - 3D-printer v05" by Creative Tools is licensed under CC BY 2.0. Accessed on 4/6/2024 <https://openverse.org/image/3cb86388-6454-4db4-8c76-bc964be88822?q=3d%20printer>

Since the main site of bone metastasis is trabecular bone, the scaffolds should be designed to mimic select features of this type of bone. Healthy human trabecular bone has been found to have a distribution of pore diameters between 5 and 950 μm ¹⁵. Recent studies measuring osteoinduction on 3D scaffolds of various pore sizes have reported better performance in scaffolds with pore diameters of 500 and 600 μm than scaffolds with both smaller and larger pore diameters²⁴. Further studies, including those studying the MC3T3-E1 cell line, have shown poor cell growth and ossification when scaffold pores are below 300 μm in diameter³⁴. Design parameters for scaffolds designed to model select properties of healthy human bone should include a pore diameter range of 300-950 μm with a recommended mean pore diameter between 500-600 μm . The geometry of the scaffold should be lattice-like to mimic trabecular bone and possess curves or obtuse angles that create ecliptic surfaces²⁵²⁶. To model late-stage cancer, it is important to also understand the effects of cancer and treatment on trabecular bone. Thus, a needed feature of a bone model would be to incorporate the states and process of osteoporosis.

When ceramic/polymer biomaterials were 3D printed, temperature was shown to be the most influential factor affecting the structural integrity of the completed print. It was also noted that in TCP/PL composite filament, the viscosity of the material increased with the mass percentage of TCP. While low mass percentage (10%) TCP/PL filaments have been extruded with a dual screw extruder and used in a commercial 3D printer showing promising results, higher mass percentage (60%) TCP/PL implants facilitated far better cell/material interactions than 30% TCP implants *in vitro*, with *in vivo* studies indicating that at 60% TCP, implants had similar biological performance to pure TCP. These results indicate that high mass percentage (>50%) TCP/PL composite scaffolds may perform just as well as pure TCP scaffolds while incorporating the properties of PL that allow it to be used in 3D printing. Studies still need to be conducted to determine whether commercial 3D printers can produce porous scaffolds with similar properties to trabecular bone using.

TCP/PL composite polymers with over 25% mass TCP need to be characterized before and to determine if TCP induces hydrolytic cleavage of PL chains to a significant degree. Significant degradation of PL would cause both the thermal stability and mechanical properties of the composite biomaterial to diminish, making the high mass percentage TCP composite material a poor candidate for use in commercial 3D printers. Additionally, previous studies on TCP/PL composites have shown conflicting results on how the addition of TCP affects the glass transition temperature of the composite at mass concentrations below 50% TCP. After using a method to produce the composite such as solvent casting, DSC analysis could provide evidence of whether or not the addition of TCP changes the thermal properties of the polymer at high mass percentage (>50%) TCP without thermal processing or mechanical work.

If the polymer shows no change in its thermal properties after the addition of TCP through solvent casting, it should be tested whether is possible to extrude 3D filaments out of the high mass percentage TCP composite biomaterial and use them in a commercial 3D printer. Subsequently, it should be verified whether structures as small and complex as a 3D scaffold for bone tissue engineering can be printed. During filament extrusion, the composite material will be heated above the melting temperature of the PL component while mechanical work is done on it by a large screw. During 3D printing the filament will again be heated above its melting as it is extruded through a brass nozzle. The effects of these processes should be taken into account when using the experimental filament to produce scaffolds as the process of extruding and 3D printing the composite could potentially produce changes in the material's mechanical or thermal properties that would need to be verified again with DSC. Additionally, compression testing of printed samples can be used as a method of assessing PL degradation at high concentrations of TCP, as a significantly degraded polymer would have a significantly lower compress modulus. It should be noted that 3D FDM printing cannot easily produce samples of solid material, and any subsequent thermal and mechanical processing done on the printed material may affect the results of compression testing. For this reason, porous compression samples should be printed directly and the effective compression modulus should be used as it accounts for the porosity of the samples.

As seen in Figure 1.3, it is important that the melting temperature of the filament material is reached as the gears push the solid filament through the heating element, but that the filament is cooled enough as it is extruded that it becomes a solid. There is a heat sink inside most printers that helps dissipate heat so that the filament can stay solidified as the gears grip and push it through the printer head and into the heater block. A thermo-sensor reads the temperature of the

heater block so that the heating cable provides the correct amount of electrical energy. As the filament melts inside the printer and becomes a fluid, it is pushed out the heated brass nozzle by the solid filament above. It is important to consider how temperature affects the viscosity of the melted composite, as TCP introduction has been shown to increase the viscosity of TCP/PL composites at lower mass percentages. This could be due to the large, solid TCP particles creating additional resistance to the flow of the melted polymer in addition to increasing the overall density of the composite.

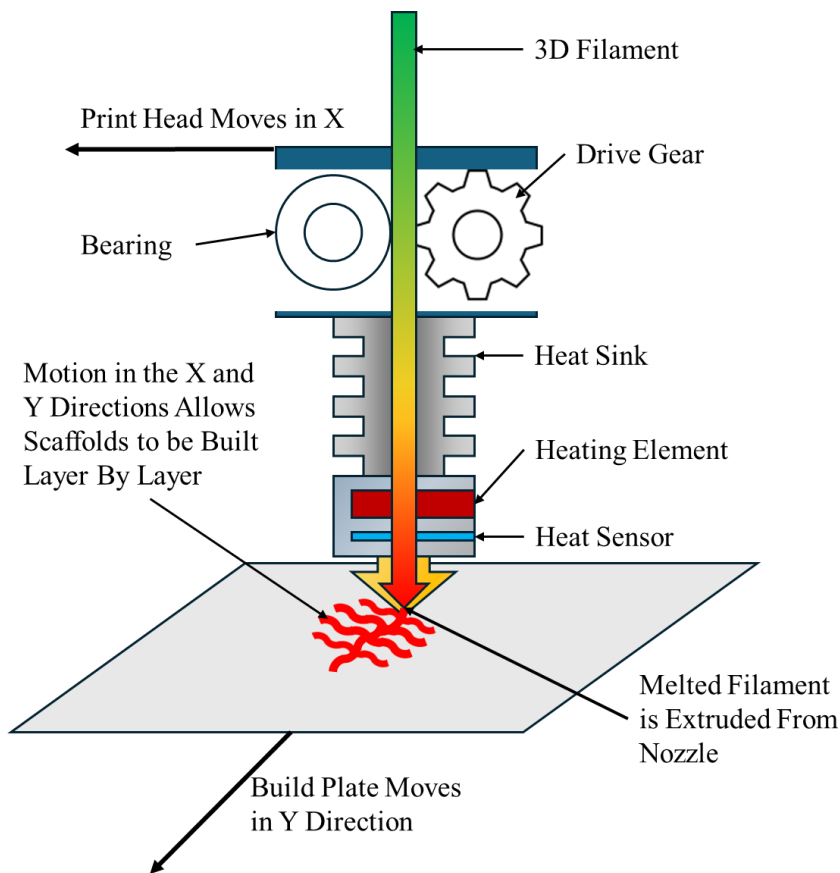


Figure 1.3: Diagram of a typical 3D printer head detailing components and motion that could create a scaffold.

Commercial off-the-shelf (COTS) 3D printers are printers available to the commercial public. As opposed to custom-built or specialized printers, they are mass-produced and often

designed to be user friendly. These printers are able to move in the X and Y directions simultaneously through a combination of stepper motors, belts, and linear guides. As COTS can have very precise movement in these directions, it is possible to print structures even as finely detailed as a scaffold.

If the composite material is capable of being manufactured into scaffolds that mimic select features of human bone, analysis of cell/material interactions including bone cell adhesion and proliferation would offer insights into its effectiveness as a model.

Hypothesis, Research Questions, and Objectives

The process to actualize the above opportunity to create new scaffolds through 3D printing is organized as an engineering design hypothesis, including requirements of the design, objectives of the work, and the subset of research questions entailed by the objectives.

Engineering Design Hypothesis

It is proposed that PL/TCP composite scaffolds, designed to model select features of the porous structure of human trabecular bone in a tissue test-system, can be fabricated using COTS 3D FDM printers in a manner that doesn't affect the thermal and mechanical properties of the scaffold to a significant degree. The scaffold should have a lattice structure that emulates specific characteristics of human trabecular bone, promotes cellular proliferation exceeding that of a control sample. ,.

Objectives and Research Questions

- 1. Show that the thermal characteristics of TCP/PL composites are not significantly changed by high mass percentages (>50%) of TCP to assess the composite's potential use in commercial 3D printers. How does the addition of TCP to PL and mechanical work done by printing influence the thermal behavior of the composite material?**

2. Demonstrate that 55% by mass TCP composite can be extruded as a filament. **Can a 55%TCP by mass composite PL filament be reliably extruded?**
3. Design two groups of scaffolds that have a curved, lattice like structure with interconnected pores that have diameters of 300-950 μm & 300-1200 μm that can be successfully printed with composite filament in a COTS 3D FDM printer. **What is the impact of using different 3D printers and printing parameters on the pore size of TCP/PL scaffolds?**
4. Demonstrate the effect that the scaffolds' geometry and pore size have on cell adhesion and demonstrate that the composite scaffolds promote higher cell proliferation than a traditional 2D culture or PL scaffolds. **Does pore diameter and porosity affect cell adhesion? Does the composite have superior proliferation to PL?**
5. Conduct mechanical testing to determine the effective Young's modulus of TCP/PL samples to see if the addition of TCP changed the mechanical properties of the PL. **Does TCP treatment enhance the mechanical properties of scaffolds fabricated from PL or possibly degrade the PL and thus reduce them?**

A flowchart detailing the scope of this work is shown in Appendix A.

Significance of the Study

This study holds significance in advancing the field of bone tissue engineered models of the human bone niche by analyzing the design, fabrication, and performance of PL/TCP composite scaffolds. The outcomes of this research may contribute to the development of more effective models of the human bone niche and potentially provide more data for the development of 3D tissue engineered bone grafts.

CHAPTER 2

COMPOSITE CHARACTERIZATION AND SCAFFOLD PRODUCTION

It is important to first establish that the proposed composite of PL and TCP is a viable material from a scaffold manufacturing perspective. Recent data published analyzing the thermal properties of TCP/PL composites suggested that TCP may enhance thermal degradation reactions of the PL³¹. If analysis of the thermal properties of the composite determines that inclusion of TCP does in fact change the thermal properties of the material, it would suggest that high mass percentage TCP/PL is a poor candidate for bone modeling. If it is determined that the presence of TCP does not significantly influence the degradation of PL, DSC data including the melting temperature can be used to select settings for filament extrusion and 3D printing.

Following analysis of the thermal properties of the material, it must be demonstrated that the composite can be extruded into a filament at a high mass percentage of TCP and that the diameter of the filament is homogeneous enough for use in commercial, off-the-shelf 3D printers. In the 3D printer class of interest, the volume of printed material is controlled by the feed rate of the polymer filament, having assumed a constant filament diameter. Thus, the filament must be extruded with minimal variability (such as a range of $<200\mu\text{m}$) in the diameter so that it will not cause variation in the amount of material printed. Successful optimization of the extrusion and 3D printing process will allow different models to be tested. Using a combination of SolidWorks and slicing software, models can be designed to mimic select properties of human trabecular bone including a curved, lattice-structure with pores between $300\text{-}950\mu\text{m}$ for healthy bone and $300\text{-}1200\mu\text{m}$ for osteoporotic.

Composite Material Preparation

Material Preparation

The composite material was prepared by weighing 9 grams of PL pellets and then placing them inside a 600mL glass beaker alongside a stir bar. The beaker was then placed inside a chemical fume hood where 200mL dichloromethane (DCM) was poured inside the beaker to dissolve the beads. DCM is a slightly polar solvent that dissolves polar plastics (the stir bar is coated with Teflon, a non-polar plastic). To reduce evaporation, labeling tape was used to cover the top of the beaker. A magnetized hot plate was set to 35°C while rotating the stir bar at a speed of 200rpm for 10 minutes. This caused the PL beads to dissolve into a slurry.

TCP sourced from Sigma Aldrich (product number: 21218) was used for this work. Received as a powder, 11 grams of the TCP powder was measured out in a weigh boat, thus establishing the desired 55/45 mass ratio with PL. After removing the tape, the powdered TCP was added to the slurry with an additional 100mL of DCM. The tape was reapplied, and the mixture allowed to sit on the hotplate while stirring until all the TCP had mixed into the slurry (usually after 5 minutes). The tape was then removed, and the temperature increased to 45°C (above the 39.5°C boiling temperature of DCM) to evaporate the solvent. A schematic of the

process is shown in Figure 2.1: Photos of the material preparation process.

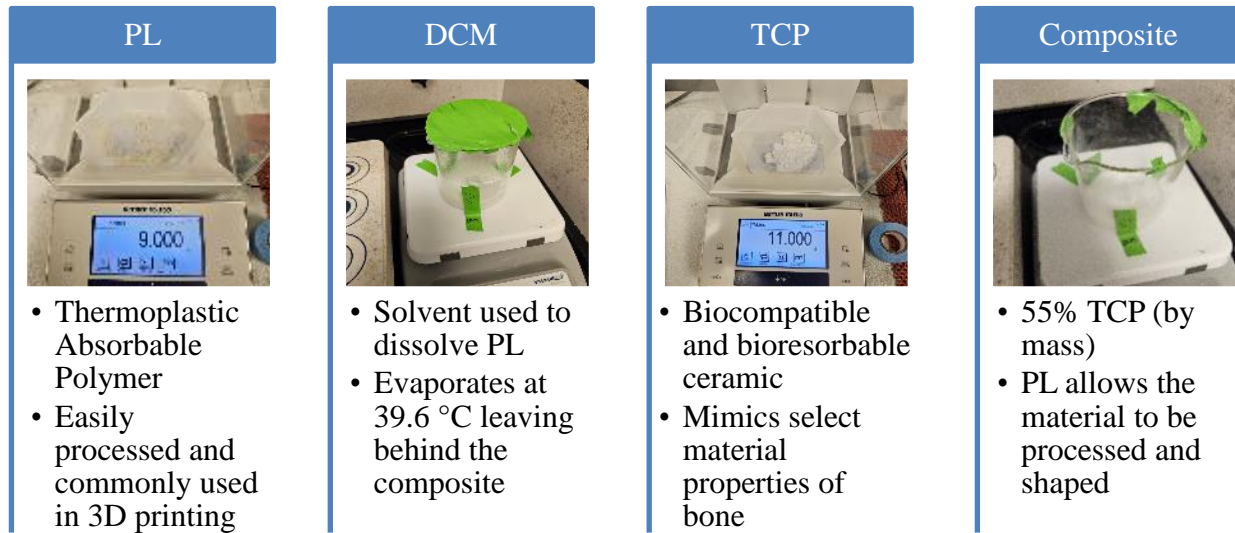


Figure 2.1: Photos of the material preparation process.

Two sample groups were prepared: pure PL pellets (as received), and 55% TCP composite. After preparing the composite to get the first state (composite as prepared), successful extrusion and subsequent 3D FDM printing was used to create the next state of TCP (post printing). By analyzing select thermal properties of the pure polymer, a baseline is produced to allow comparison of the two states of composite, output of composite preparation and output of the 3D printer, to see if the introduction of TCP and the processing required to produce a scaffold affected the thermal properties of the polymer.

Thermal Characterization

Differential Scanning Calorimetry (DSC) is a commonly used analysis for determining the thermal properties of a material. Specifically, DSC measures heat flow associated with transitions in materials as a function of temperature using thermocouples.

The purpose of using Differential Scanning Calorimetry (DSC) on samples of tricalcium phosphate (TCP) and polylactide (PL) composite was to characterize the thermal properties of

the composite biomaterial and to determine if the addition of TCP altered the thermal characteristics in any significant way. PL (as seen below in Figure 2.2) is among the most common polymers used in 3D printing and has also widely been studied as a biomaterial in 3D cell culture. As some studies^{32,31} have suggested that TCP may play a role in the thermal degradation of PL even at lower mass percentages, it should be evaluated if the addition of high mass percentages of TCP does cause any form of degradation within the range of temperatures needed for filament production and 3D printing.

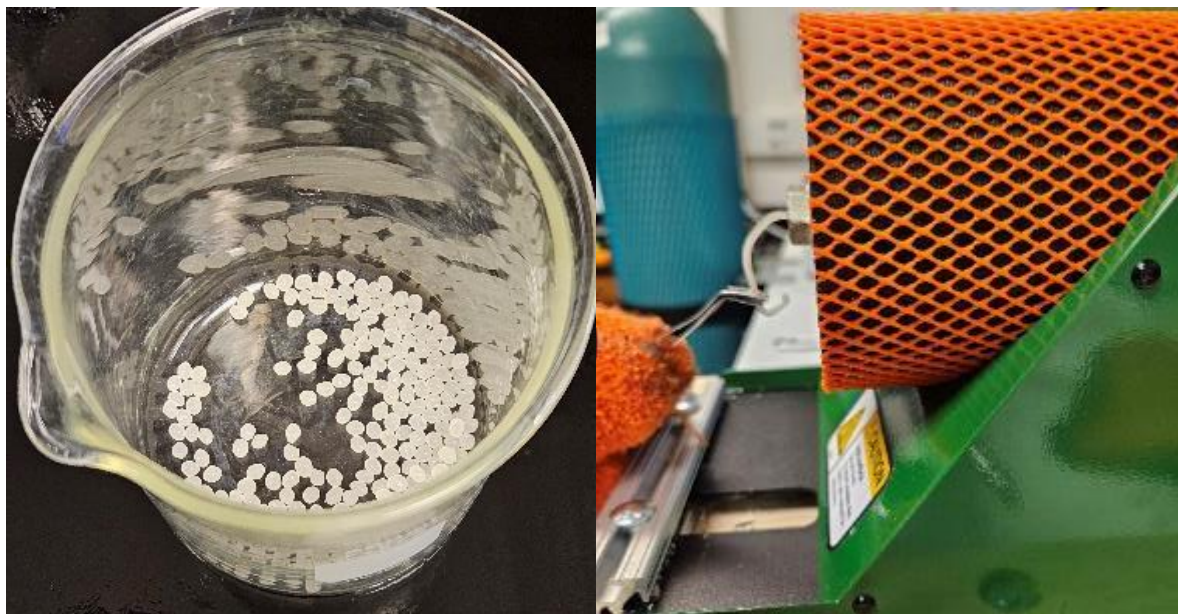


Figure 2.2: Left - As received PL pellets. Right - PL fiber after extrusion.

DSC samples needed to be small enough in shape and volume that they would fit into a 1 mg aluminum pan. PL samples were created by taking as received PL pellets and carefully cutting them with a razor blade. A crucial aspect of sample preparation was the determination of sample mass. Samples were weighed in a weigh boat using an electronic scale. It was imperative that the mass of each sample fell within a range of 5 to 20 milligrams to comply with the operational limits of the Netzsch Polyma 214 Differential Scanning Calorimeter.

The weighed samples were then loaded into aluminum sample pans. An aluminum lid was placed on top of the pans and pressed down with a Netzsch DSC 3500 Sirius to form an airtight seal. An additional empty pan was also pressed together as a control sample. A small hole was then poked into the lids of both pans to allow any gases released during heating to escape.

Thermal Analysis

The DSC analysis of the composite samples was carried out using the Netzsch Polyma 214 Differential Scanning Calorimeter. The Netzsch Polyma 214 uses an oval furnace to heat samples and then measures the samples with ring-shaped sensors and has a reported Indium Response Ratio of over 100 mW/K. The machine also allows heating and cooling rates of 0.001 K/min to 500 K/min.

The DSC procedure involved heating the material from 25°C to 200°C at a rate of 20°C per minute. After quenching to 25°C, samples were left idle at temperature for 10 minutes. After reheating at the same rate, samples were left idle at 200°C for one minute. All samples were run for four cycles, using nitrogen gas to purge the chamber. These settings were based on specifications detailed in the literature³¹.

Of the three sample groups, two were initially prepared for DSC analysis. As received PL pellets and 55% (by mass) TCP/PL composites were prepared as the initial two sample groups. Three samples were tested from each group, and thermograms were subsequently plotted in Proteus® thermal analysis software to determine whether the melting temperature and glass transition region were significantly different. All data was collected from the fourth cycle of each run. Data was exported from the Proteus® software following analysis, and example plots were made in Microsoft® Excel based on single-point raw data.

A statistical analysis was conducted on the data to compare select thermal properties. The following equation (Equation 1) was used to calculate the degree of crystallinity (X_c) for each sample:

$$X_c = \frac{\Delta H_f - \Delta H_c}{\Delta H_f^0(1 - \theta)} * 100$$

Equation 1. ΔH_f is the enthalpy of fusion, ΔH_c is the enthalpy of cold crystallization, ΔH_f^0 is the enthalpy of fusion for 100% crystalline PL (93.6 J/g), and θ is the mass fraction of TCP in the composite.

Results and Discussion

A comparison of Figure 2.3 and Figure 2.4 reveals a lack of a crystallization peak in both the samples. The glass transition regions and endothermic peaks appear to be at the same temperatures as well. This result agrees with previous studies characterizing the thermal behavior of lower mass percentages of TCP/PL composite^{31,32}. Of note, however, is the lack of crystallization in both the as received PL and the TCP/PL composite. As received, the polymer was not oriented and therefore might not have any crystallinity³⁵. The fact that the 55% by mass TCP composite material did not crystallize suggests that the TCP particles did not act as crystallization sites for the polymer as one might expect. Based on the thermograms, the method used to combine the polymer and TCP particles into a composite material (DCM solvent) did not cause the polymer chains to reorient themselves in any way that would change their crystallization behavior either. Following the extrusion and printing processes, three samples of 3D printed composite were collected and analyzed just as the two sample groups before were.

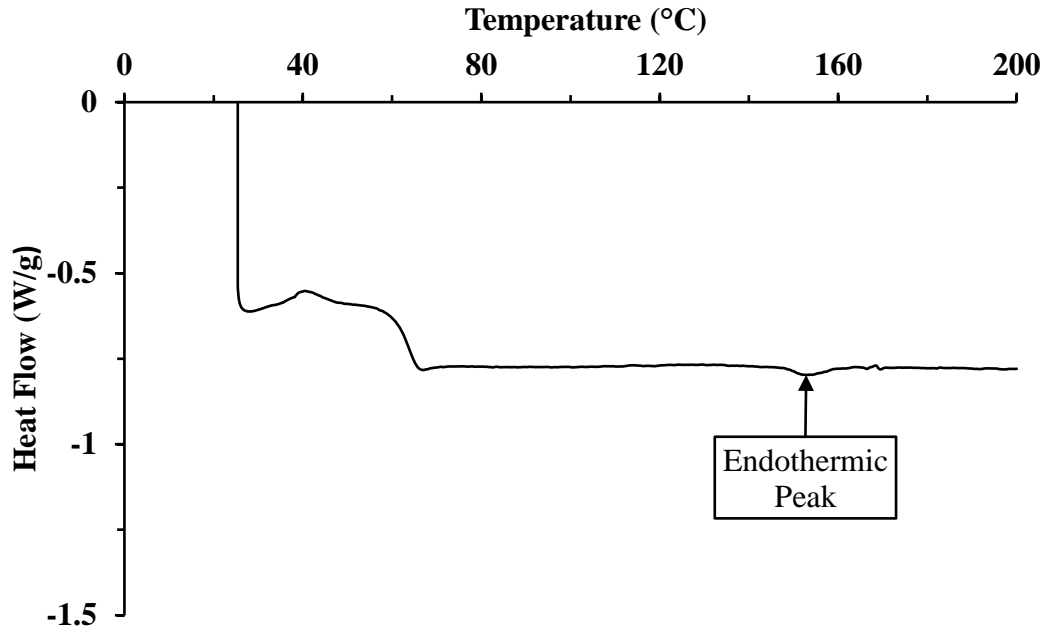


Figure 2.3: DSC thermogram of a 6mg sample of pure PL.

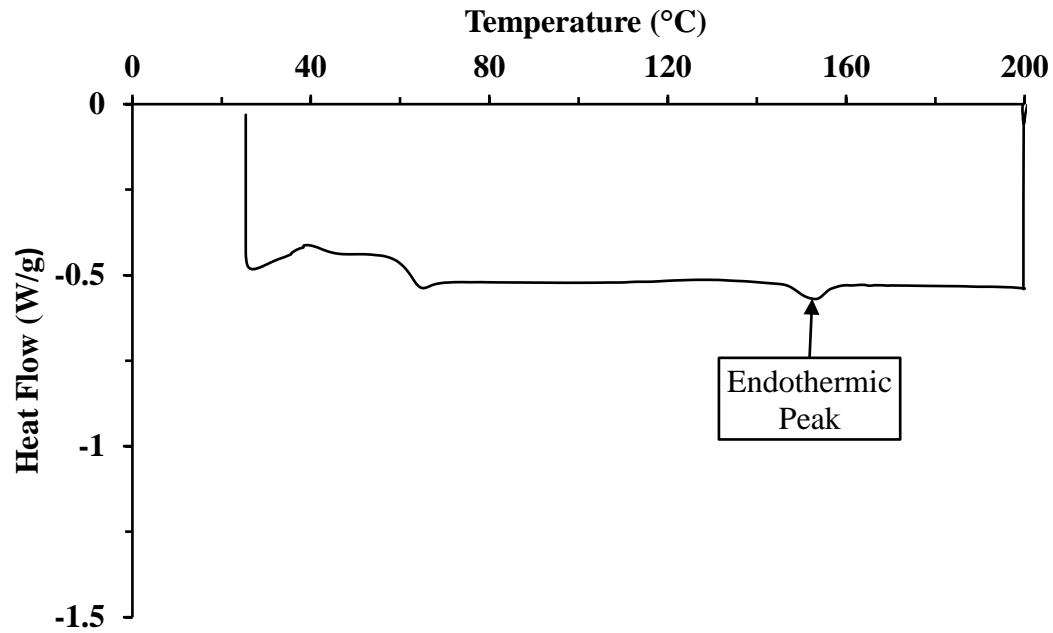


Figure 2.4: DSC thermogram of a 10mg sample of 55% TCP/PL composite as prepared.

As seen in Figure 2.5, the printed composite now has a crystallization peak and a sharper endothermic peak indicating the PL experienced cold crystallization inside the DSC. The

orientation of polymer chains is known to affect whether or not the material exhibits crystallization³⁵. The crystallization of the printed composite is likely due to mechanical work done on the composite by the extruder and the 3D printer appears to cause the polymer chains to reorient, allowing crystallization.

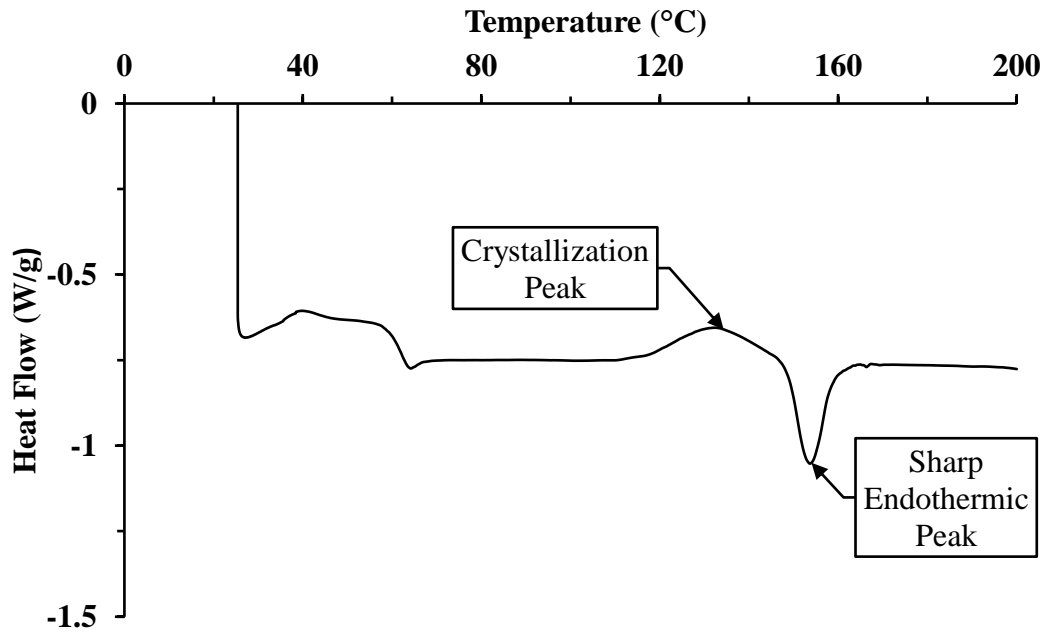


Figure 2.5: DSC thermogram of 10mg sample of printed 55% TCP/PL composite

Table 2.1

ANOVA statistics for fourth cycle DSC data^a for pure PL, 55% TCP by mass composite as prepared, and 55% TCP by mass composite after filament extrusion and 3D printing.

Dependent Variable	Source	DF ^b	F-Stat ^c	p ^d > F
T_m	Material	2	0.6328	0.5632
T_g	Material	2	3.52	0.097
T_g (Onset)	Material	2	4.7459	0.0581
T_g (End)	Material	2	1.7559	0.251
ΔH_c	Material	2	16.50	0.004

ΔH_f	Material	2	11.36	0.009
$\Delta H_f - \Delta H_c$	Material	2	83.85	0.00004
X_c	Material	2	55.97	0.0001

^a Null hypothesis (H_0): The source of variability is zero.

^b Degrees of Freedom

^c Sum of Squares

^d Mean Square

^e Fischer statistic

^f Probability of observing results as or more extreme assuming a correct null hypothesis

As seen in the far-right column of Table 2.1, the p-value for melting temperature (T_m) is higher than the significance level threshold of 0.05. This means that within the 95% confidence interval, we cannot reject the null hypothesis that the addition of TCP has no statistically significant effect on the melting temperature of the samples tested. Similarly, the glass transition onset ($T_{g(O)}$), midpoint (T_g), and endpoint ($T_{g(E)}$) all have p-values above a 0.05 threshold. This indicates that at the 95% confidence interval we cannot reject the null hypothesis that 55% TCP has zero effect on the melting temperature or the glass transition range of TCP/PL composites. This result is supported by previous studies that evaluated lower TCP mass percentage composites and garnered similar results^{31,32}.

The p-values for the enthalpy change for cold crystallization (ΔH_c) and the enthalpy of fusion (ΔH_f) both were far below a confidence threshold of 0.05. As expected, based on visual inspection and comparison of Figure 2.4 and Figure 2.5, analysis suggests there is a statistically significant difference in the crystallization behavior of the material after processing. The p-value for the original heat of fusion ($\Delta H_f - \Delta H_c$) was extremely small ($p < 0.0001$) suggesting that there was a statistically significant difference in the amount of crystallinity present in the material before heating. The range of values for the original heat of fusion were much smaller in the processed 55% TCP composite than either the PL or the unprocessed composite. The same is true

for the degree of crystallinity; while the p-value is extremely small ($p < 0.0001$), the printed composite had the lowest degree of crystallinity. This suggests that while the extrusion and printing processes caused cold crystallization to occur, it simultaneously reduced the number of crystals in the PL prior to DSC analysis. This could be due to pressure and mechanical work done on the composite during extrusion and printing processes that caused the polymer and TCP molecules to rearrange.

Overall, the statistical analysis indicates that the introduction of TCP particles and subsequent processing to produce a 3D printed scaffold does not have a statistically significant effect on the thermal properties of the composite outside of its crystallization behavior. These results show no evidence that would suggest against the use of high mass percentage TCP/PL composite filaments for 3D FDM Printed scaffolds for the purpose of modeling human bone.

Filament Extrusion

The process of filament extrusion included demonstrating that the composite could be extruded using a Filabot EX2 and determining the optimal extrusion parameters to ensure a uniform filament that can be successfully 3D printed.

Methods

The screw extruder used for filament production was a Filabot EX2 extruder with a standard 1.75mm nozzle.

As with the material prepared for DSC analysis, as received PL pellets were weighed to determine mass. The pellets were dissolved into a beaker containing DCM and stirred with a Teflon coated stir bar. After the pellets were completely dissolved, powdered TCP was added to the slurry and the temperature was increased to evaporate the DCM. To break the material into a size small enough to load into the hopper of the screw extruder, pieces were broken up by hand

(while wearing gloves). To facilitate easy breaking of the composite, a wide beaker (600mL) was used so that the produced composite disc would be thinner.

The initial temperature used for filament extrusion was 185°C, the manufacturer recommended temperature for PL filament extrusion. This temperature was found to produce filament that while homogenous, would create outliers in certain sections (some greater than 2.00mm in diameter) that could potentially clog printers designed for 1.75mm filament. Previous studies have recommended lower temperatures for extrusion of TCP/PL filament to account for changes in viscosity, and so the temperature of extrusion was lowered³¹. As temperatures were lowered, it was found an extrusion temperature of 165°C produced filaments with uniform diameter while ensuring that no outliers were so large that they would clog a commercial 3D printer or so small that they would easily break. Of note, an extrusion temperature of 165°C is over 10°C above any melting temperature collected during DSC analysis of the composite material ensuring that any of the minor fluctuations in temperature the FilabotEX2 may be prone to during the extrusion process do not cause any part of the material to decrease below its melting temperature.

While extruding at the same setting, extrusion speed would often fluctuate based on the amount of material inside the extruder. To accommodate for this, the extrusion setting was manipulated during extrusion to ensure the screw was rotating at approximately 3 rotations per minute.

First, the screw extruder was checked to make sure it was firmly placed on a flat surface. The cord was plugged into the wall, and the power switch was flipped. Once the power was confirmed on, the temperature control was switched on. The temperature was set to 165°C and

the machine was allowed to heat until it reached 165°C (usually taking about 5 minutes if the machine was empty beforehand).

Once the machine was fully heated, small pieces of TCP/PL composite were loaded into the hopper at the top of the machine. The extruder was turned on to move all the pieces into the main chamber where they would be heated; the extruder was then turned off and the machine was then left to melt the material for 5-10 minutes.

The only variables that can be directly controlled by user input on the screw extruder are temperature, and (to a lesser extent) the extrusion speed. Once the material inside the main chamber was given time to melt, the extruder was turned on again at a speed of approximately one full rotation every three seconds. Even at the same setting on the machine, extrusion speed can vary based on the amount of material loaded into the extruder and these variables were kept the same to ensure consistency among filaments extruded. As the filament was pushed through the die, it was carefully picked up with tweezers and gently lifted to create a filament that was as straight as possible. The resulting filament was entirely opaque and solid white in color (like the feedstock).

To analyze the filament diameter, measurements were taken at every inch with a digital caliper. Measurements were taken at 90° rotations around the filament to ensure that any ovality of the filament was considered, and if there was any discrepancy, an average of the lowest and highest value measured were taken. After measuring three separate filaments at ten locations one inch apart, a one-way ANOVA analysis was conducted on the data collected to assess the hypothesis that the three filaments are homogenous in diameter.

Results and Discussion



Figure 2.6: An extruded filament being measured; units are in centimeters.

An image of the finished filament can be above in Figure 2.6. This demonstrates that 55% TCP by mass composite material can be extruded into a filament using a commercial screw extruder such as the FilabotEX2.

Table 2.2

ANOVA statistics for diameter analysis^a of 55% TCP composite filament composite extruded at 165°C.

Dependent Variable	Source	DF ^b	SS ^c	MS ^d	F-Value ^e	P-Value ^f
<i>D</i>	Between Groups	2	0.0003	0.0002	0.2317	0.7948
	Within Groups	27	0.019	0.0007		
	Total	29				

^a Null hypothesis (H₀): The source of variability is zero.

^b Degrees of Freedom

^c Sum of Squares

^d Mean Square

^e Fischer statistic

^f Probability of obtaining results at least as extreme as those observed

The results of the one-way ANOVA analysis in Table 2.2 provide evidence that the filament diameter remains consistent between filaments. The P-value of 0.7948 shows that at the 95% confidence interval the null hypothesis cannot be rejected. This provides evidence to support the null hypothesis that the diameter of the composite filament is uniform when extruded under previously described conditions.

Scaffold Design and 3D Printing

Printer Selection

The initial design chosen for testing whether a printer can extrude the composite filament into any kind of scaffold was a square lattice structure created using SolidWorks AutoCAD software. The test scaffolds were designed to have 400 μ m by 400 μ m struts with 400 μ m gaps between the struts. The struts were layered to create a 1cm by 1cm cube. While recent studies^{26,27,29} suggest that a square lattice structure's 90° angles would adversely affect cell adhesion, it was hypothesized that these models would be easy to print in high fidelity and thus a good model to test the capabilities of various printers.

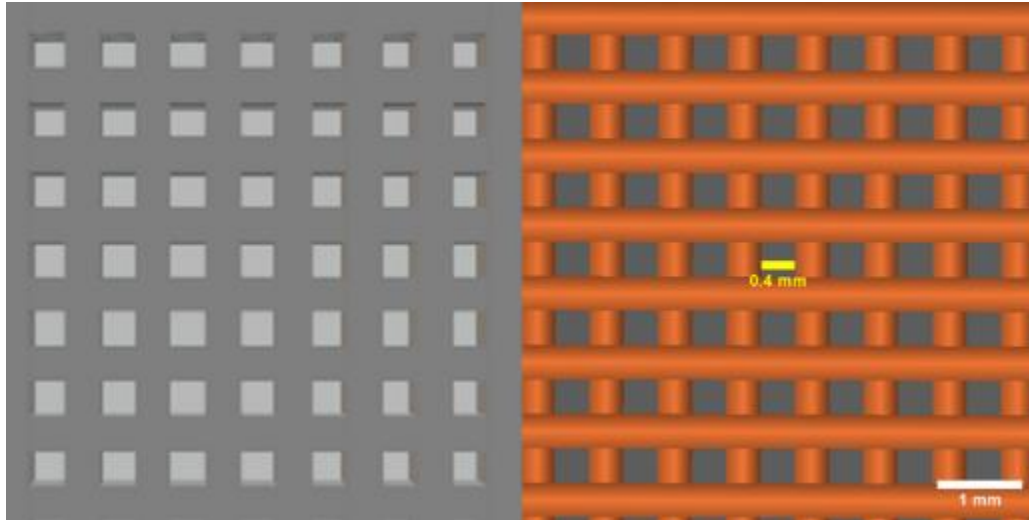


Figure 2.7: Right-Top view showing the first two strut layers of a lattice structure showing struts were spaced $400\mu\text{m}$ apart.

The three printers tested were the PrusaMK3S with a 0.4mm nozzle, Dremel DigiLab 3D45 with a 0.2mm nozzle, and a Monoprice Ultimaker with a 0.3mm nozzle. All three printers were able to print the lattice structure in PL. This was expected as all three printers were designed to use PL filament.

Following printing the lattice structure with PL, the composite biomaterial filament was used in all three printers to produce a lattice scaffold. For the Dremel this required bypassing the chip reader using an empty spool of PL filament and feeding the composite directly into the printer. While all three printers could successfully extrude the filament, the Ultimaker had frequent issues with layer adhesion that could not be mended with more optimal printer settings in the CURA slicer software. Dremel was able to partially print the lattice structure in composite filament, but its fidelity was extremely poor. The PrusaMK3S on the other hand was able to extrude a full height scaffold after modifications to its slicer software although issues with layer attachment occurred frequently. Lowering the PrusaMK3S's extrusion temperature to 195°C , the

first layer temperature to 205°C, and allowing Z-hopping solved issues where layers would sometimes detach. The final result can be seen below in Figure 2.8. It was therefore established that going forward, the PrusaMK3S would be used.

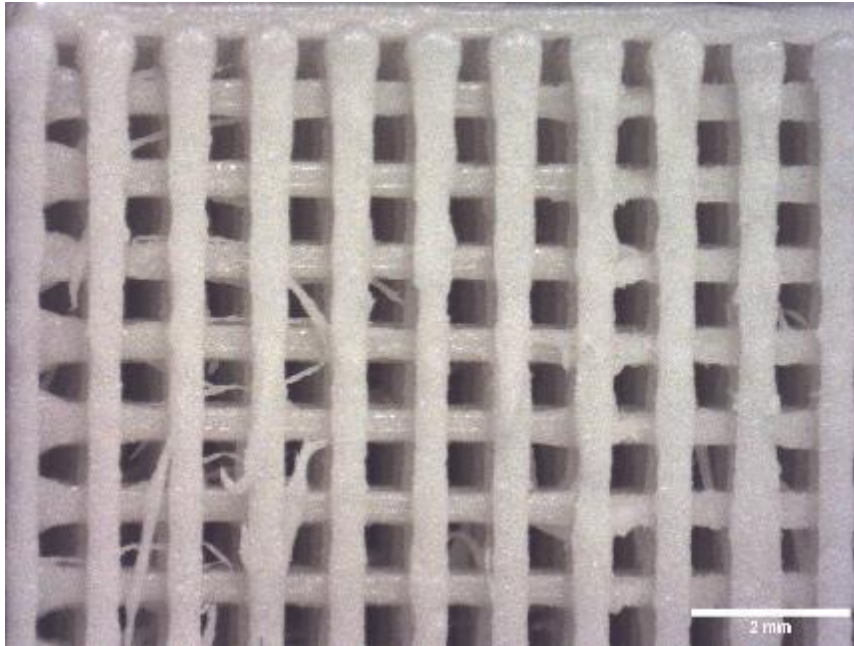


Figure 2.8: Composite lattice structure printed with a PrusaMK3S.

Scaffold Design

Once it was established that a simple structure like a square lattice scaffold could be printed with high fidelity in composite, further designs were created to model the properties of trabecular bone derived from literature review. These design parameters include a curved pore face with interconnected pores possessing diameter ranges of 300-950 μ m were selected. in AutoCAD and exported to the PrusaSlicer. Each test scaffold was designed to have dimensions equal to one cubic centimeter. An example of how scaffolds were designed to model select properties of trabecular bone can be seen below in Figure 1.1

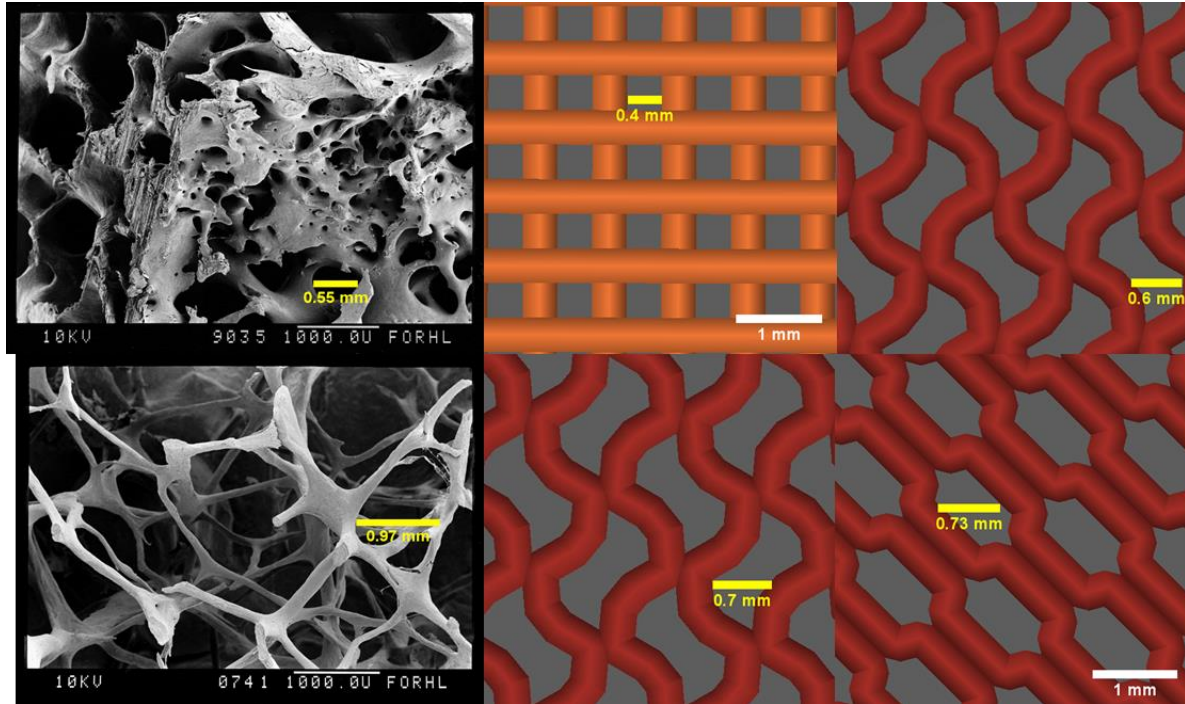


Figure 2.9: Top Left- Healthy trabecular bone. Bottom Left- Osteoporotic bone with trabecular distance. Top Center- Two strut levels of the square lattice in PrusaSlicer. Bottom Center- bottom layer of the gyroid geometry produced with 50% infill setting in PrusaSlicer. Top Right- bottom layer of the gyroid geometry produced with 60% infill setting in PrusaSlicer. Bottom Right- bottom layer of a hexagonal 60% infill pattern. (Credit: SEM bone, sawn surface + fracture face. SEM old osteoporotic bone. David Gregory & Debbie Marshall. Modified by Brett Ritchey (addition of pore measurement). Attribution 4.0 International (CC BY 4.0). Source: Welcome Collection. Accessed 4/3/2023 at <https://wellcomecollection.org>.)

The designs included a gyroid structure that was made in 3DSMax, a scaffold with 300 μ m cylindrical pores between each face, a scaffold with 300 μ m hexagonal pores between each face, and a cube made to use the native infill settings on the PrusaMK3S available in the PrusaSlicer. Of these native infill settings, the gyroid infill and honeycomb infill were used on

the cube to create a model with a porous structure. As infill directly correlates to porosity, the infill percentage could be used to estimate the porosity of the final print.

After designing the models, commercial PL filament was used to determine whether or not they could be printed. The 3DSMax gyroid was unable to be sliced correctly in the PrusaSlicer and was therefore abandoned. All test models were printed using 0.20mm layers and default settings for PLA filament. For both the gyroid and honeycomb infill models, infill was set to 50%, 60%, and 70% and the layers of vertical and horizontal shells that would cover the outside of the print were all set to zero to create an exposed pore surface.

After slicing the model and turning it into G-code for the PrusaMK3S, the models were printed. The only models that successfully printed with an intact pore structure were the Prusa's native infill settings. Post printing, a stereoscope at 0.75x magnification was used to image the scaffolds so that the number of pixels in an image taken could be directly related to the dimensions of the object imaged based on a previous image taken of a calibration sample. The calibrated values on the stereoscope were then used to set the scale in ImageJ analysis software. Based on the number of pixels in the line, the actual pore size could be measured. Measurements were made perpendicular to the direction of the struts to ensure accurate diameter measurements. The results of printing can be seen below in Figure 2.10.

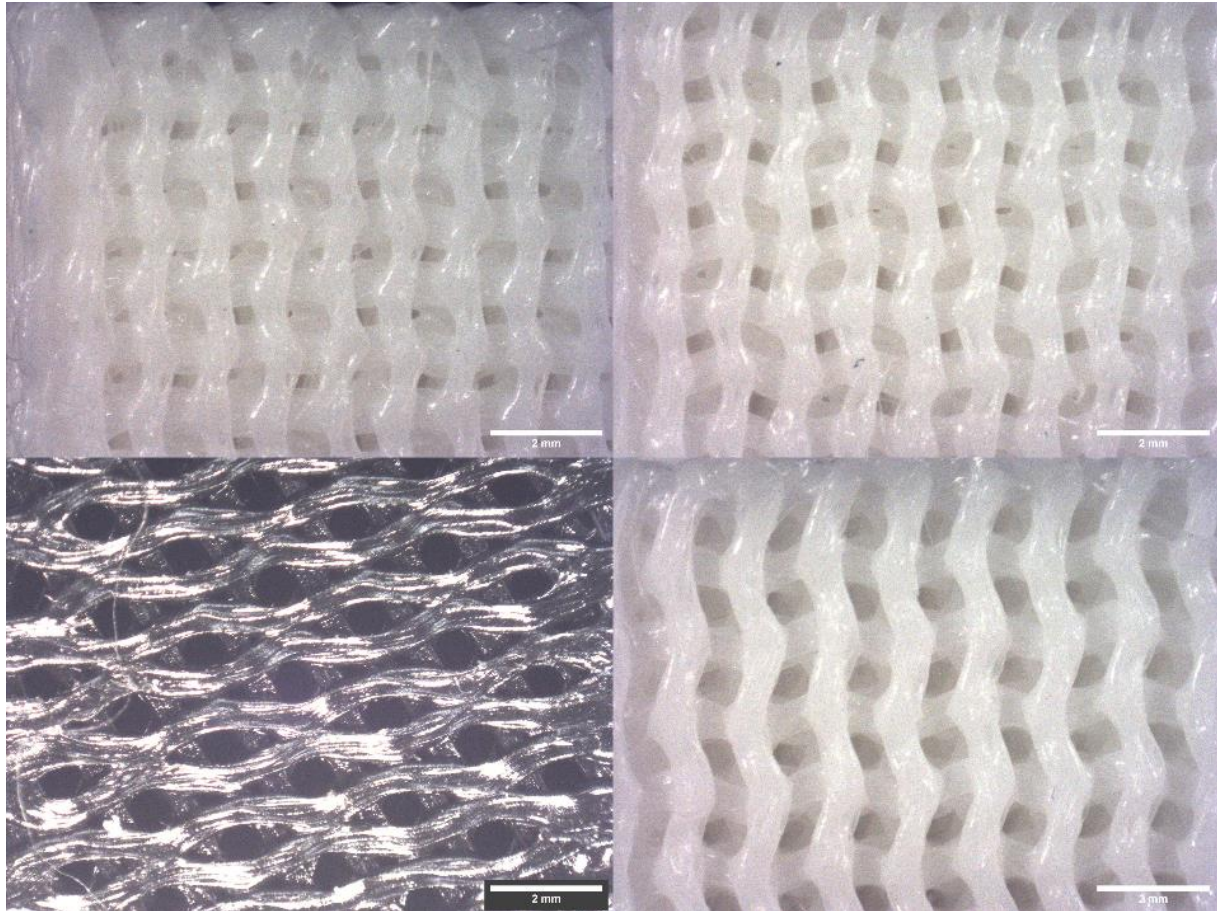


Figure 2.10: Top Left- PL scaffold produced with 70% gyroid infill. Bottom Left- PL scaffold produced with 60% hexagonal and black filament. Top Right- PL scaffold produced with 60% infill. Bottom Right- PL scaffold produced with 50% gyroid infill.

The conclusions drawn from pore measurement were that only the gyroid infill structure could create a curved surface in a lattice like structure with interconnected pores of the desired diameters. The honeycomb infill scaffolds had little to no pore interconnectivity after printing while others with perfectly round pores could not be printed. Settings of 50% gyroid infill (for osteoporotic) and 60% gyroid infill (for non osteoporotic) were determined to be the only scaffolds to meet the design criteria that could be printed as the 70% gyroid infill produced pores below the 300 μ m.

After deciding on the pore structure, scaffolds were designed that could fit into a 48-well plate. The dimensions of the 48-well plates used were such that the scaffolds needed to be cylindrical and have a diameter of 9.9mm. The height of the scaffolds was set to be 5mm so that they could be covered with sufficient media. A cylindrical structure with these specifications was created in AutoCAD and imported to the prusa slicer. Top views showing the pore structure of the sliced scaffold models can be seen below in Figure 2.11 and Figure 2.12. A side view showing the dimensions of the scaffold and porosity of the side can be seen in Figure 2.13.



Figure 2.11: Top view of a 50% gyroid infill model in the PrusaSlicer software showing pore structure.

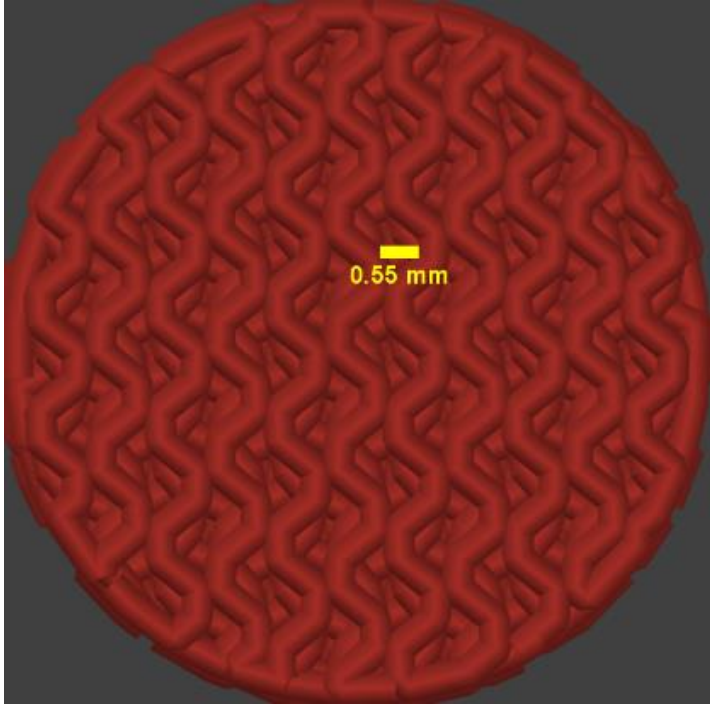


Figure 2.12: Image of a 60% gyroid infill model in the PrusaSlicer software showing pore structure with intended pore diameter.

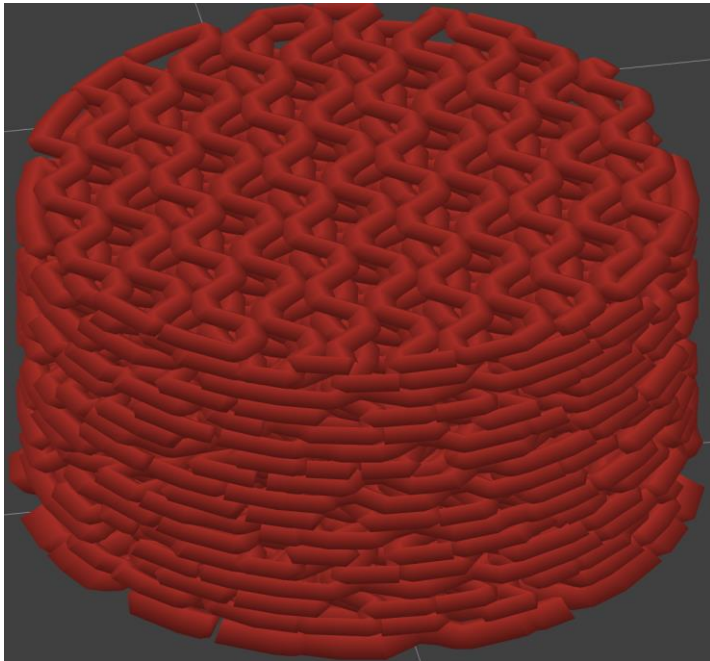


Figure 2.13: Oblique top and side perspective of a sliced scaffold; the sides are porous as well.

Results and Discussion

Stereoscopic images of the fully printed scaffold can be seen below in Figure 2.14 and Figure 2.15, where layers of waveform struts are layered across each other to create a pore geometry similar to a gyroid. Summary statistics from the results of these measurements could then be calculated and Welch's two sample t-test was performed to test if the samples had the same means.

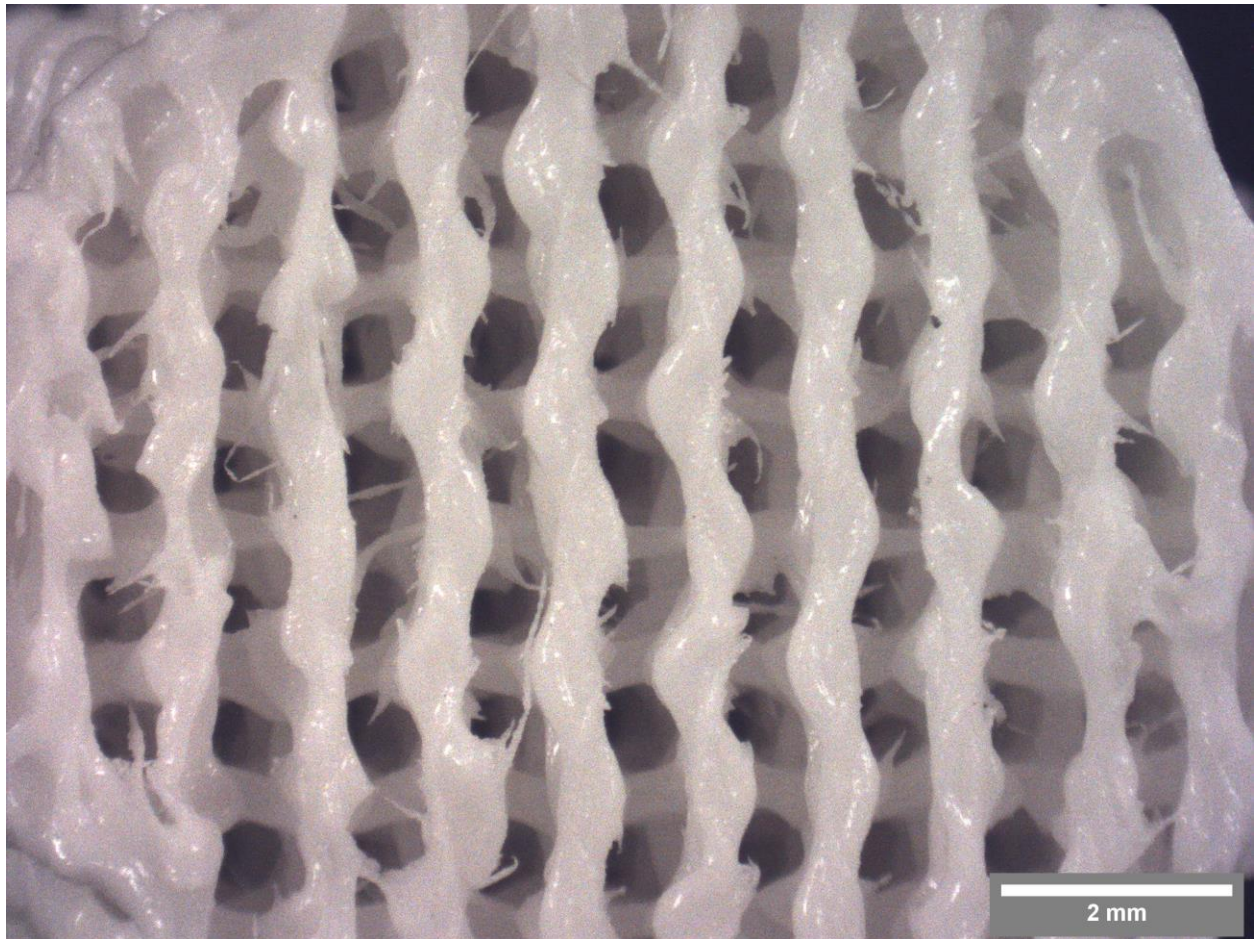


Figure 2.14: Top view of a composite scaffold produced with 60% infill setting with scale bar, taken by stereoscope.

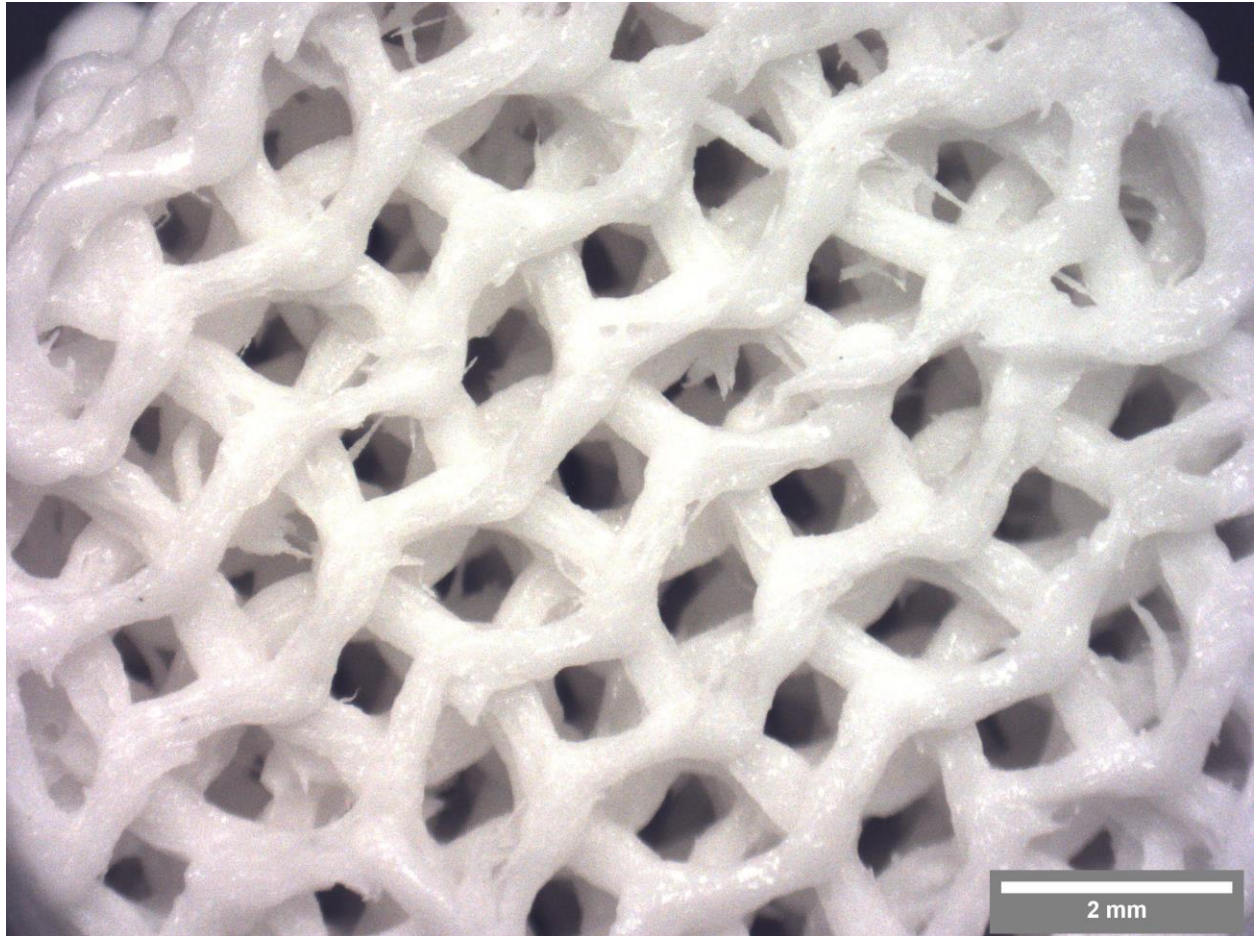


Figure 2.15: Top view of a composite scaffold produced with 50% infill showing pore structure with scale bar, taken by stereoscope.

Figure 2.14 demonstrates that a PrusaMK3S can produce a scaffold with curved, interconnected pores in the desired range using 55% TCP by mass PL composite filament. Figure 2.12 shows a computer rendered model of the scaffold prior to printing. Comparison of these two images shows that the model was printed successfully and with high fidelity to the computer model.

Similarly, comparing Figure 2.15 to Figure 2.11 one can see that a 50% infill setting can also produce a scaffold with high fidelity to its sliced model using composite filament. The 50% infill scaffolds show a visibly larger pore

size than the 60% infill scaffolds, indicating that these scaffolds have a higher porosity and are therefore more suitable for simulating an osteoporotic bone environment.

Table 2.3

Summary statistics for diameter analysis of 55% TCP composite scaffolds. All units are in μm .

Dependent Variable	Source	\bar{x} ^a	S ^c	Min ^d	Max ^e
D	60% Infill	553.6	93.5	330	780
	50% Infill	839.3	215.3	400	1200

^a Mean

^b Standard deviation

^c Minimum pore diameter

^d Maximum pore diameter

As seen in Table 2.3, the range of the pore diameter (D) of the 60% infill group (330-780 μm) falls within the desired range selected to mimic the pore size of human bone (50-950 μm). Additionally, it means the engineering design criteria for healthy bone tissue scaffolds, having a minimum pore diameter above 300 μm and a mean between 500 and 600 μm . The range of the 50% infill scaffold (400 μm -1200 μm) does not. It does, however, fall within the desired criteria for modeling osteoporotic bone. It should be noted that the standard deviation of the 50% infill scaffold ($\pm 93.5\mu\text{m}$) was over twice that of the 60% infill scaffold ($\pm 215.3\mu\text{m}$). It can be said that based on this value, the 50% infill scaffold has a much lower printing fidelity than the 60% infill scaffold.

There were roughly two thirds the number of pores in the 50% infill scaffold as opposed to the 60% scaffold despite both having the same area suggest otherwise. If one further inspects the minimum and maximum values of both groups, it is apparent that the 50% infill group can produce minimum values (400 μm) similar to the 60% group (330 μm). The maximums of both groups, however, are entirely different. The 50% infill group's maximum value of 1,200 μm is

much higher than the 60% infill group's maximum value of 780 μm . This puts the 50% infill group outside the pore size range of health human bone (5-950 μm).

Table 2.4

Welch's t-test for scaffold diameter^a of 55% TCP composite filament composite extruded at 165°C.

Dependent Variable	Source	CI ^b	T-Stat ^c	P-Value ^e
<i>D</i>	Between Groups	[-0.25586 0.13383]	-6.5309	1.055E-8

^a Null hypothesis (H₀): The source of variability is zero.

^b Confidence Interval

^c Test statistic

^d Probability of obtaining results at least as extreme as those observed

The results of Welch's T-test shown in Table 2.4 include a P-Value of 1.0545E-08. This P-value is far below the significant level of 0.05 used for the confidence interval. This statistical analysis suggests that the two samples have statistically significant differences in pore size.

Both the mean and standard deviation for the 60% infill group suggest that all of its pores are likely to fall within the pore size range of normal healthy human bone. This provides evidence that the 60% infill model is a strong candidate for modeling healthy human bone. Similarly, the standard deviation and pore size of the 50% infill group show that it may be an effective model of osteoporotic bone. The mean pore diameter in the 50% infill group (839 μm) is higher than that of healthy human bone, but a pore size that large could be expected in osteoporotic bone. Like osteoporotic bone, the 50% infill group still contains pores within the range of healthy human bone. This indicates that the 50% infill group is a strong candidate for modeling osteoporotic bone or breast-cancer to bone metastasis.

Mechanical Testing

Sample Preparation

As with the cell scaffolds, the PrusaMK3S 3D printer was used to produce the mechanical testing samples. The compression samples used for mechanical testing included PL alone and TCP/PL samples produced with the 60% infill setting along with three additional layers on top and bottom to create a flat surface. The chosen gyroid infill pattern was expected to provide structural integrity while maintaining a porous architecture similar to trabecular bone like that used in the scaffolds.

Each sample was designed to be flat on both the top and bottom surfaces, ensuring uniform loading during compression testing. The dimensions of each cylindrical sample were as follows:

- **Height:** 1 cm
- **Diameter:** 0.5 cm

The composite samples were composed of polylactide (PL) and tricalcium phosphate (TCP) at a 55% TCP by mass ratio. The composition was selected based on earlier experiments and the expectation that the high mass ratio of TCP could yield favorable mechanical properties.

The samples were grouped according to their material composition (PL/TCP with 55% TCP by mass) to facilitate a direct comparison with samples composed of pure PL, enabling a comparison to determine any significant differences in their effective Young's modulus.

Methods

A Mark-10 Compression Tester set for compression testing was used to acquire mechanical testing data. The machine functions by compressing samples mounted between the upper and lower platens. As force is applied to the sample, the force, time, and displacement of the upper platen is recorded.

Mechanical testing occurred at a constant compression rate of 1.3mm/min. Each specimen was compressed until breakage occurred. Testing was conducted in a dry state to

ensure that water did not affect the results of the test. Each sample was placed in the center of the lower platen.

The force and displacement data for both PL and PL/TCP scaffolds were collected through the Mark-10 compression tester. Each of the two groups comprised five samples to ensure sufficient sample size. As soon as the machine measured a total pressure above one Newton, force (N), time (s), and displacement (mm) data were set to automatically be collected.

To determine the effective Young's modulus, the force data was divided by the estimated surface area of the top of the scaffold to determine the stress. The displacement data was then used as a fraction of the initial length of the scaffold (1cm) to calculate the strain. This data was plotted using Microsoft excel software, and visual inspection was used to determine the linear region of the graph. An example can be seen below in Figure 2.16.

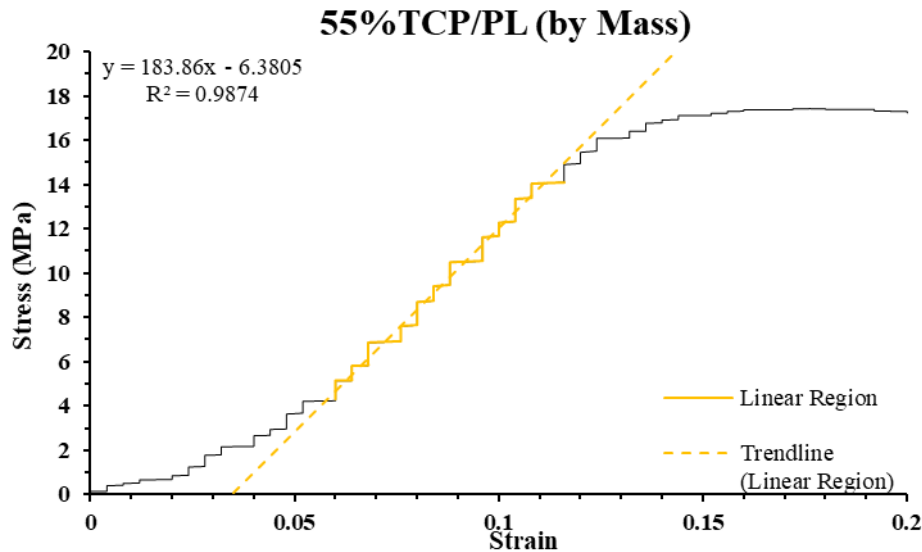


Figure 2.16: Graph of a 55% TCP compression sample.

Quality control measures were implemented to ensure consistency among the produced samples. The 3D printing process was closely monitored to avoid variations in layer deposition thereby minimizing internal defects that could affect the results of mechanical testing. Samples

with defects observed during printing were disposed of. To further confirm a lack of internal defects in the composite scaffolds, their weights were taken prior to compression. It was determined that there was no statistically significant difference between any of the scaffolds based on a confidence interval of 95% and a sample size of 5.

Before mechanical testing, the samples' surfaces were characterized using stereoscopic imaging to confirm the intended flat top and bottom surfaces lacked any holes, as well as to verify the overall integrity of the printed structures. Additionally, an extra sample was printed to the halfway point before stopping the printer to confirm the porous internal structure was printed as intended. As FDM printers work by layering molten filament in prespecified patterns and all samples used the same pattern, it was expected that the main source of surface roughness would be caused by the FDM printing method and based on the round deposition of the nozzle would be relatively uniform across samples. Still, to minimize variation due to the characteristics of the compression surface, non-parametric statistical analysis should be used.

As seen in Figure 2.17, the bottom of the compression sample was flat as intended. Figure 2.18 shows that the interior portion of the compression samples was successfully printed.

To ensure reproducibility and reliability, all scaffolds were printed with the same printer. Samples for each group were compressed using the same machine with the same settings. Samples from each group were produced from the same filaments (55% TCP and PL).

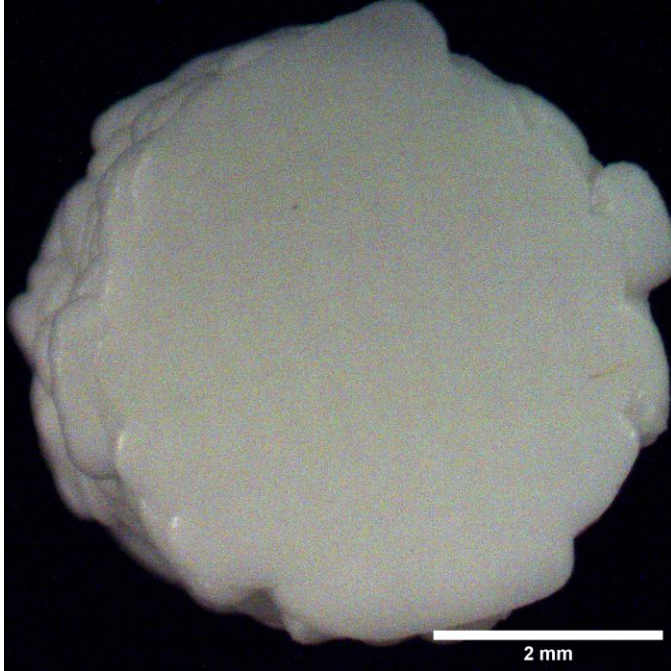


Figure 2.17: Stereoscopic image of the compression surface of a composite sample.

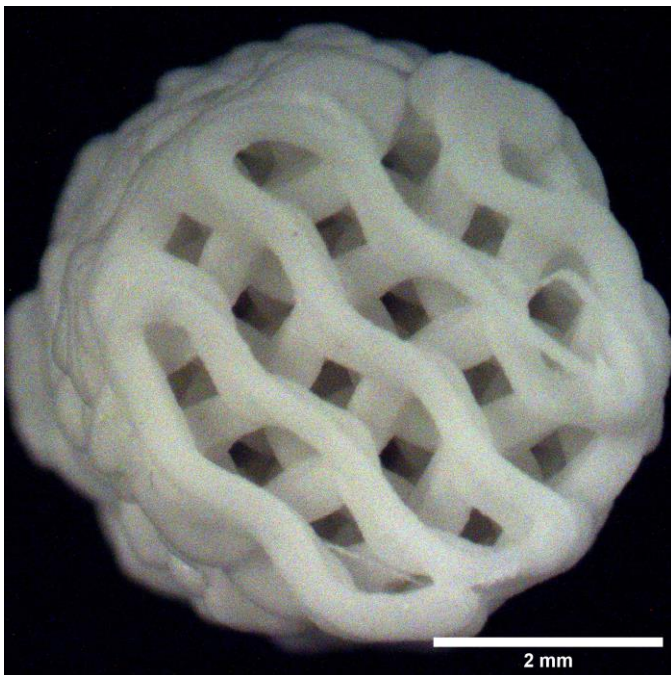


Figure 2.18: The interior portion of a compression sample.

Results and Discussion

As seen in Figure 2.19, the mean effective compression moduli (E) of the composite compression samples are visibly dissimilar, but not by much. Composite samples display a noticeably lower mean than the pure PL samples and a much wider standard deviation. The PL samples had an effective Young's Modulus of 169.35 MPa, a value 32.48 MPa above and 123.7% of the composite samples' effective E of 136.87 MPa. TCP/PL composites of 25% mass ratio have been documented as having a similar E to pure PL while 5 and 10% TCP by mass samples had a higher E ³¹. It was speculated that a lower E (and thus a change in mechanical properties) was due to TCP catalyzed thermal degradation of the polymer composite during manufacture in a hot press.

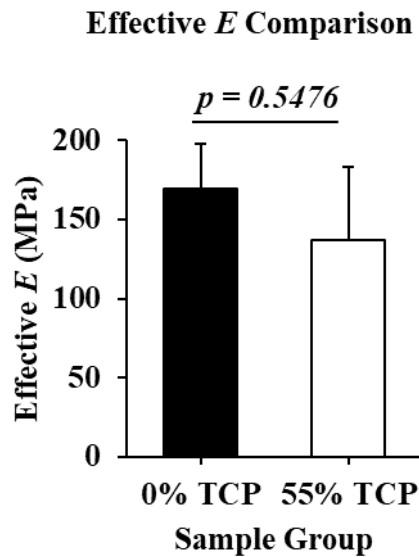


Figure 2.19. Comparison of effective E for samples of pure PL and 55% TCP/PL compression samples.

A Mann-Whitney U-test was run on the effective Young's Moduli of both groups to determine if there was significant difference between them. The p-value calculated derived from the test was 0.5476. This value is much larger than the significance level of 0.05, thus the null hypothesis that there is no difference in Effective Young's Modulus between the groups is not

rejected. We cannot reject the null hypothesis that there was zero difference and conclude that TCP treatment and post processing altered the mechanical properties of PL based on the results of this statistical analysis.

The results of mean compression testing show that TCP/PL composite scaffolds appear to be the same or slightly weaker than PL scaffolds in terms of effective E , while the statistical analysis proves inconclusive. This study gives no evidence to support the hypothesis that TCP treatment of PL catalyzed thermal degradation reactions during printing to the degree that they would significantly alter the mechanical properties of the material. If there is little to no degradation due to the process of printing the scaffolds, TCP/PL can be used at mass ratios of 55/45 in 3D printing without harming the tissue test system.

A limitation of the compression testing is that the 3D printing process cannot consistently produce 100% solid material and additional processing after 3D printing could further alter mechanical properties. For this reason, only effective E testing can be conducted. To remedy this, scanning electron microscopy (SEM) of printed samples could reveal to what degree degradation of the biopolymer may have affected its surface better than mechanical testing and assays could be used to evaluate harmful bioproducts of degradation released.

CHAPTER 3

CELL/SCAFFOLD INTERACTIONS

Following successful development of scaffolds with select properties to mimic human trabecular bone at different stages of metastasis, cells can be used in experiments to observe whether they interact with the scaffolds as expected.

While there are four primary types of bone cells, osteoblasts can differentiate into mature osteocytes. In the same way, immature pre-osteoblasts can differentiate into osteoblasts. For this reason, a single cell line may be used to assess the cell/material interactions of the scaffolds. The MC3T3 cell line of pre-osteoblastic mouse cells are one of the most common osteoblast-like cell lines used in osteogenic evaluation³⁶ and are therefore a perfect candidate for assessing cell/scaffold interactions. A combination of adhesion testing and an alamarBlue™ assay should allow preliminary characterization of how the MC3T3 cells interact with the scaffold. It is expected that the 60% infill scaffolds will have a higher number of cells adhered than the 50% since the pores on these scaffolds more closely mimic properties of the trabecular bone environment. It is also expected that the composite scaffolds will facilitate greater cell proliferation as TCP has been shown to enhance the activity of bone cells in other TCP infused composite biomaterials.

Cell Adhesion Experiments with MC3T3 Cells

Methods

This section details the methodology employed for seeding MC3T3 cells onto the fabricated scaffolds and subsequent cell number estimation with a hemocytometer. The adhesion

experiments used eight scaffolds in total, with four scaffolds printed with PL using the 50% gyroid infill setting and four scaffolds printed with PL using the 60% gyroid infill setting. The purpose of this study was to determine which of these scaffolds allowed better cell adhesion, the 50% infill (which represents osteoporotic bone) or the 60% infill (which represents healthy bone) and to compare both to a positive control group so that estimations can be made about cell adhesion in future experiments.

PL scaffolds were used in this experiment as extensive research³⁷ exists on the surface treatment of 3D FDM printed PL, ensuring that results are based on pore geometry alone and not surface characterization. Prior to seeding, the surfaces of the scaffolds were treated with an NaOH and deionized water solution for thirty minutes. The NaOH solution decreased the hydrophobicity of the polymer in the scaffolds by roughening the surface of the polymer in the scaffold. Chemically, this involves the strong base cleaving the ester bonds in the polylactide polymer chains.

MC3T3 media, PBS, and trypsin were warmed before starting the procedure. Conical tubes (15mL), a waste beaker, a 100-1000 μ l pipette, and a 20-200 μ l pipette were all used. All materials were placed inside the BSC after being sprayed with ethanol. After removing the medium from the flask using an aspiration pipette tip, 3mL of PBS were pipetted into the flask and the flask was gently shaken for 1 minute. Afterwards, the PBS was replaced with Trypsin-EDTA solution, and the flask was placed in the incubator for 5 minutes. After tapping the bottom of the flask, the Trypsin-EDTA cell suspension was then pipetted into a conical tube with 10mL of complete media (89% EMEM, 10% bovine serum, and 1% antibiotic solution) to neutralize the trypsin. A 20 μ L sample was taken for measurement by hemocytometer before the conical tube was then centrifuged at 1200rpm for 5 minutes. The total cell number was estimated with a

hemocytometer. After aspirating the medium from the centrifuged cells, the pellet was diluted with the MC3T3 medium so that there were ~500,000 cells per 1mL and there was more than 1 mL of cell suspension. A volume of 50uL (25,000 cells) of the cell suspension was pipetted onto each scaffold by placing the pipette directly above the top center of the scaffold and dispensing the liquid. The 50µL volume was selected based on a pilot study that determined this volume would be distributed throughout as much of the scaffold as possible (mainly the top/center) but would not cause any leakage. The cell suspension was vortexed between scaffold seedings to ensure as equal a distribution of cells as possible. The same volumes (and therefore number of cells) were pipetted into 4 wells inside a tissue-treated 24-well plate. After 60 minutes in the incubator, 500µL of media was added to each well and deionized H₂O was added to the surrounding wells to prevent evaporation. The well plates were returned to the incubator. The remaining cells that were not seeded were dispensed into a new flask for future experiments.

After 24 hours of incubation, a new non-tissue treated 48-well plate was placed in the BSC. The cylindrical scaffolds were gently placed into the new non-tissue treated 48-well plate with fine-point tweezers. The outer edge of the scaffold was grabbed to avoid disturbing the cell-surface. A volume of 500uL PBS was placed into each of the wells containing scaffolds and the plate was gently shaken by hand for 1 minute.

The PBS was completely drained from the wells using an aspiration pipette. The eight scaffolds were submerged in 500uL trypsin/EDTA solution. The well plate was placed back into the incubator and onto the shaker. The shaker was set to 7 and the well plate was shaken for 8 minutes.

While the well plate was being shaken, eight conical tubes (15mL) were labeled inside the BSC, each with the alpha-numeric designation of a different scaffold.

After 8 minutes had passed, the scaffolds were transferred back to their previous wells, taking care not to spill any trypsin out of the wells. The trypsin solution (containing cells) was drained from each of the wells into eight 15mL conical tubes. A volume of 4.5mL of medium was added to each conical tube. Each of the tubes were vortexed before drawing 20uL for cell counting.

Results and Discussion

A graph of the results of the cell counting can be seen below, in Figure 3.1. The control sample had a mean estimated cell number of 26,250. As it is expected that 100% of cells would adhere in the tissue treated cell culture, this shows the methods of seeding were precise.

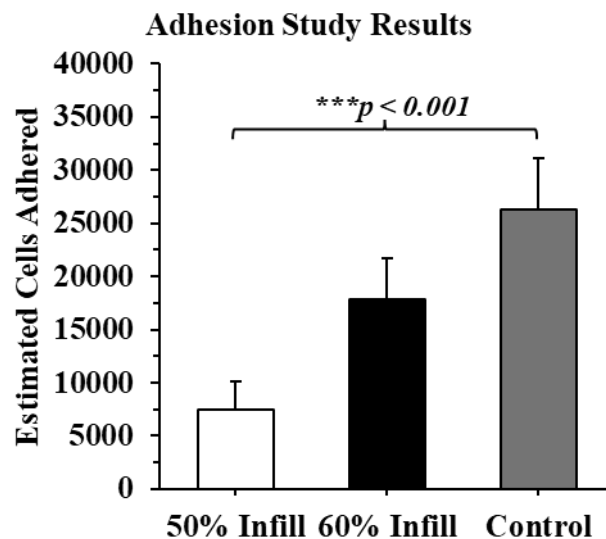


Figure 3.1: Adhesion study results showing the number of cells adhered to the scaffolds.

There was a large visible difference in the number of cells adhered to each of the scaffolds seen in this figure, where 67.86% of the estimated cell numbered adhered to the 2D cell culture were estimated to have adhered to the 60% infill scaffolds. For the 50% infill scaffolds, this number was 28.57%. A subsequent statistical analysis was conducted on the estimated numbers.

Table 3.1

Statistics for cell adhesion^a of MC3T3 cells onto porous scaffolds made of pure PL.

Dependent Variable	Source	DF ^b	SS ^c	MS ^d	F-Value ^e	P-Value ^f
<i>n</i>	Between Groups	2	705468750	352734375	23.1538	0.000283
	Within Groups	9	137109373.9	15234374.9		
	Total	11	842578123.9			

^a Null hypothesis (H₀): The source of variability is zero.^b Degrees of Freedom^c Sum of Squares^d Mean Square^e Fischer statistic^f Probability of obtaining results at least as extreme as those observed

An Analysis of Variance (ANOVA) test was conducted to assess whether there are statistically significant differences in the number of cells adhered (*n*) among the three groups. The results of this analysis can be seen in Table 3.1. The p-value of 0.000283 indicates highly significant.

A Post-hoc Tukey-Kramer test was then performed to identify which groups are significantly different:

1. Comparison between 50% Infill and 60% Infill:

- p-value: 0.0001
- Difference: -1.8018 (in 1.0e+04 units)
- Upper Bound: -1.0312 (in 1.0e+04 units)

2. Comparison between 50% Infill and Control:

- p-value: 0.0002
- Difference: -2.6456 (in 1.0e+04 units)
- Upper Bound: -1.8750 (in 1.0e+04 units)

3. Comparison between 60% Infill and Control:

- p-value: 0.0003
- Difference: -1.6143 (in 1.0e+04 units)
- Upper Bound: -0.8438 (in 1.0e+04 units)

This test confirmed that in comparisons between each group, the p-values were all smaller than 0.001, indicating a highly statistically significant difference between each group tested. The negative differences in each of the above comparisons indicates that the 50% infill group had statistically significantly less cells adhered than the 60% infill group and that the control (as expected) had a significantly higher amount of cell adhesion than either of the PL scaffold groups.

These results are in line with the initial hypothesis behind the experiment. The results of this experiment provide evidence to support the hypothesis that a pore size closer to that of healthy human bone supports cell adhesion of MC3T3 cells better than a pore size larger than human bone.

Cell Viability and Proliferation with MC3T3 Cells

Methods

This experiment included six composite scaffolds (55% TCP by mass, three 60% infill and three 50% infill) and a group of three 60% infill PL scaffolds. In contrast to the adhesion study, cells were seeded at 10,000 cells per scaffold using the same volume (50 μ L) of a more dilute cell suspension.

Cells were seeded in the same fashion as in the adhesion study, except that instead of two groups of PL scaffolds, there were three groups of scaffolds. Extruded TCP/PL composite

filaments have been shown to have greatly increased hydrophility³¹ compared to PL alone. As with the adhesion study, PL scaffolds were treated for 30 minutes.

After the cells were incubated for 24 hours to allow ample time for cells to adhere to scaffolds, the alamarBlue™ assay was conducted. A vacuum aspiration pipette was used to remove all of the medium from the scaffolds and the positive control group (the 2-D tissue-treated cell culture) while care was taken not to press the aspiration pipette tip anywhere near the cell surface (center of the scaffolds). Inside a BSC, the scaffolds were carefully transferred with tweezers from the non-tissue treated 48 well-plate they were incubated in and into sterile non-tissue treated 24 well-plates. To avoid touching the cell-surface, only the sides of the scaffolds were grabbed with tweezers. With the lights inside the BSC turned off, 15mL of media was combined with 1.5mL of ThermoScientific™ alamarBlue™ Cell Viability Reagent inside a 50mL conical tube. The conical tube was then vortexed to mix the reagent with the media before 1mL of the solution was pipetted into each of the wells (including the positive control group). A volume of 100µL of the alamarBlue™/media solution was pipetted into six wells of a 96-well plate to form the positive control. After two hours in the incubator, 100µL of the reagent solution was pipetted from the bottom corner of the wells containing the scaffolds and the 2-D cultures and into twelve wells of a 96-well plate. The remaining reagent solution was vacuumed from the wells using an aspiration pipette. The scaffolds were washed three times with DPBS and then carefully removed and placed into a new non-tissue treated 48-well plate. Medium was pipetted into the wells to cover the scaffolds and the plates were placed in the incubator. On day three, the experiment was conducted again.

A Biotek™ Synergy™ HTX Multi-Mode Reader was used to acquire absorbance data. Using the alamarBlue™ reader profile adjusted for the samples in the 96-well plate. Readings

were taken at both 570nm and 600nm and interpreted based on instructions given by ThermoFisher™ for the reagent.

Results and Discussion

The percentage of reagent converted was calculated for each replicate and subsequent standard deviations were calculated without averaging replicates. Results can be seen in Figure 3.2.

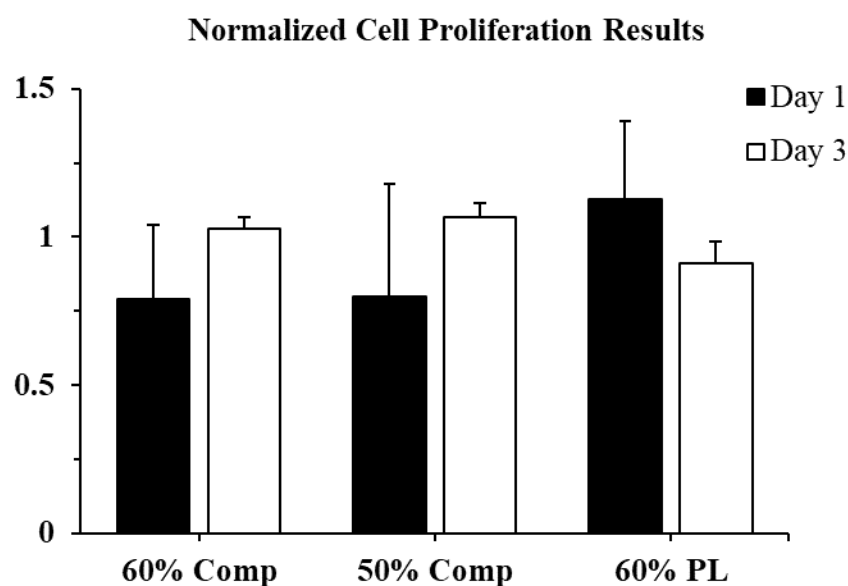


Figure 3.2: Percent alamarBlue™ normalized around averages of the control. Scaling factor for standard deviation was 0.05.

After 24 hours, the 60% infill composite samples converted roughly 79 % of the reagent that the positive control group did. It is expected that cell proliferation 24 hours after seeding would not be significant, therefore this number is mostly a representation of the cells able to adhere to the scaffold. Since the hemocytometer study estimated that 68% of cells in a 60% infill scaffold would adhere, these results follow expectations that TCP promotes higher cell adhesion. The 50% infill composite group converted 80% of the reagent the control did. As this value is

roughly the same as the 60% infill composite, it may be that the TCP treated PL surface allowed greater cell adhesion than the 50% PL scaffolds in spite of inferior pore size, but this result could also be due to a large margin of error in seeding the cells in 3D. The 60% infill PL scaffolds converted 113% of the reagent the control did. It may also be that there was a larger margin of error in the process of seeding the 3D scaffolds, as the normalized standard deviation for all groups was many times larger on day 1 than day 3. This could indicate that the cells adapted quicker to the 2D environment and proliferated more or were in a more metabolically active state than the 3D environment, or perhaps that the seeding methods employed for the scaffolds created large standard deviations that weren't seen in the adhesion study.

At 72 hours, the 60% and 50% composite groups converted respective averages of 103% and 106% of the reagent as the positive control. The 60% PL group only converted 91% of the control percentage on average. Compared to the results on Day 1, this suggests that there were more cells on the composite scaffolds than either the control or the PL scaffolds despite day 1 results indicating that both scaffolds had less cells adhered initially than either the control or the PL group. This indicates very strongly that the TCP/PL scaffolds promote much higher proliferation of bone cells than any of the other sample groups tested. These results of this experiment are mirrored in a recent study conducted on filaments made of 0%, 5%, 10% TCP/PL filaments using MG-G3 cells and an MTT assay³¹.

The results of the proliferation experiment show strong evidence that TCP/PL polymer scaffolds have the potential for enhancing bone cell proliferation, making them strong candidates for modeling the human bone niche. Future directions could include the use of human cells instead of mouse bone cells. Additional studies that focus on osteoinduction or osteoconduction of bone cells could provide further evidence of the model's effectiveness.

CHAPTER 4

DISCUSSION AND CONCLUSIONS

Summary of Key Findings

1. Detected, by DSC analysis, changes in the crystalline behavior of the composite after filament extrusion and 3D printing
2. Demonstrated that 55% by mass TCP composite can be extruded with a commercially available screw extruder and used as a filament in a commercial 3D printer.
3. Demonstrated that a COTS 3D FDM printer (the PrusaMK3S) was capable of 3D printing composite scaffolds with design parameters intended to model select features of human trabecular bone.
4. Assessed the scaffolds' bone cell adhesion and bone cell/material interactions using MC3T3 (mouse pre-osteoblast) cells and determined that 60% infill setting scaffolds had higher cell adhesion than 50% infill scaffolds and that both composite groups exhibited higher cell proliferation after three days than either the control or PL scaffold groups.
5. Conducted mechanical testing and determined that the effective Young's modulus of PL/TCP scaffolds and determined that at the 95% confidence level, a sample size of five showed no statistically significant difference in Young's modulus values indicating that TCP may not enhance the mechanical properties of the scaffolds.

Interpretation of Results

The thermal analysis indicates that the introduction of TCP does not significantly affect the melting temperature of the material. It does, however, show that the 3D printed biomaterial

crystallized after being processed. This is likely mainly due to mechanical work done on the composite during processing and not thermal degradation. Mechanical testing and statistical analysis of effective E found no conclusive evidence that the printing process affected the 3D printed samples in a way that would degrade them significantly.

The results of the cell/material interaction studies support the findings in current literature that wide angled (or curved) pore geometries like the gyroid structures printed in combination with ceramic polymer composite biomaterial allow greater cell/material interaction.

A comparison of both the cell adhesion and cell/material interaction studies show that scaffolds with 60% infill had higher cell adhesion than scaffolds with 50% infill. The scaffolds produced with the TCP containing composite filament were also shown to have significantly higher levels of cell proliferation than that of the 2-D positive control group which itself had higher cell proliferation than the 3D PL-only scaffolds.

Within the confines of bone tissue modeling, this research provides more evidence to support scaffold geometries and pore sizes already thought to promote cell adhesion and proliferation. The use of the MC3T3 cell line on scaffolds composed of 55% TCP shows that the composite biomaterial, as hypothesized, increases the proliferation of pre-osteoblasts.

Based on the results found in this work, TCP/PL composite scaffolds can be fabricated using COTS 3D FDM printers with specific design criteria to mimic select features of the porous structure of human trabecular bone in a tissue test-system. These scaffolds appeared to have higher cell proliferation than scaffolds made purely of PL or traditional 2D cell cultures, indicating that any degradation due to TCP influenced thermal degradation reactions may have increased cell proliferation or at least not hindered it more than the TCP treatment increased it.

Limitations and Future Directions

Despite significant progress in recent years involving the advancement of 3D printers and slicing software, challenges in scaffold design persist. Bone is a complex tissue with differences in vascularity and geometric properties existing not only between the broader categories of bone tissue types but even between and within individual bones themselves. Future directions could involve using more advanced 3D FDM printers to produce complex structures that currently cannot be printed.

Additionally, bioreactors have been used in tissue engineering to improve cell proliferation and seeding with patient specific tissue that include bone³⁸. Perfusion bioreactors can be made with commercially available parts and provide enclosed environments biochemically and biophysically optimized for specific types of mammalian cells. These reactors function by generating flow of specific media within a scaffold containing reactor chamber. Additionally, in bone tissue engineering, these bioreactors can be used to incubate cells with specific growth factors that promote bone cell proliferation. In these scaffolds, mineralization has shown to increase with optimized reactor flow rates³⁹. Spatial optimization techniques have also shown promising results in improving bone tissue engineering⁴⁰.

Conclusion

This research provides strong evidence that ceramic/polymer composites can be extruded into filament, even at TCP mass concentrations above 50%. It also provides strong evidence that these composite filaments can be used in COTS 3D FDM printers to produce porous scaffolds of similar pore size and geometry to human trabecular bone. Cell material interactions have shown that these scaffolds have higher proliferation rates than traditional 2D cell cultures.

The results of this work show that the PrusaMK3S is capable of producing scaffolds made from high mass percentage (55%) TCP/PL composite filament that meet all engineering design requirements. This suggests that the introduction of further bone cell lines and cancer cells could be used with these scaffolds to model the metastatic bone niche. Using advanced analytical techniques such as flow cytometry, these scaffolds could provide data on the metastatic environment, possibly resulting in new treatments or strategies for the treatment of bone metastasis.

REFERENCES

1. Siegel, R. L., Giaquinto, A. N., & Jemal, A. (2024). Cancer statistics, 2024. *CA Cancer J Clin*, **74**, 12–49.
2. Cancer Institute, N. (2020). Metastatic Cancer. *Nat. Cancer Inst.* Available at: <https://www.cancer.gov/types/metastatic-cancer> (Accessed February 3, 2024).
3. Buijs, J. T., & van der Pluijm, G. (2009). Osteotropic cancers: From primary tumor to bone. *Cancer Lett.*, **273**, 177–193.
4. Fornetti, J., Welm, A. L., & Stewart, S. A. (2018). Understanding the Bone in Cancer Metastasis. *J. Bone Miner. Res.*, **33**, 2099–2113.
5. Huang, Y., Wang, H., Yue, X., & Li, X. (2023). Bone serves as a transfer station for secondary dissemination of breast cancer. *Bone Res.*, **11**, 1–13.
6. Tsukamoto, S., et al. (2021). Current overview of treatment for metastatic bone disease. *Curr. Oncol.*, **28**, 3347–3372.
7. Ban, J., Fock, V., Aryee, D. N. T., & Kovar, H. (2021). Mechanisms, diagnosis and treatment of bone metastases. *Cells*, **10**, 1–15.
8. Pang, L., et al. (2022). Bone Metastasis of Breast Cancer: Molecular Mechanisms and Therapeutic Strategies. *Cancers (Basel)* (2022) doi:10.3390/cancers.
9. Paget, S. (1989). The distribution of secondary growths in cancer of the breast. *Cancer Metastasis Rev*, **8**, 98–101.

10. Akhtar, M., Haider, A., Rashid, S., & Al-Nabet, A. D. M. H. (2019). Paget's "Seed and Soil" Theory of Cancer Metastasis: An Idea Whose Time has Come. *Adv Anat Pathol*, **26**, 69–74.
11. Sitarski, A. M., Fairfield, H., Falank, C., & Reagan, M. R. (2018). 3D Tissue Engineered in Vitro Models of Cancer in Bone. *ACS Biomater. Sci. Eng.*, **4**, 324–336.
12. Florencio-Silva, R., Sasso, G. R. D. S., Sasso-Cerri, E., Simões, M. J., & Cerri, P. S. (2015). Biology of Bone Tissue: Structure, Function, and Factors That Influence Bone Cells. *BioMed Res. Int.*, **2015**, 421746.
13. Chang, B., & Liu, X. (2022). Osteon: Structure, Turnover, and Regeneration. *Tissue Eng. Part B Rev.*, **28**, 261–278.
14. Tahara Rie K., et al. (2019). Bone Metastasis of Breast Cancer. in *Breast Cancer Metastasis and Drug Resistance: Challenges and Progress* (ed. Ahmad, A.) 105–129 (Springer International Publishing, Cham, 2019) doi:10.1007/978-3-030-20301-6_7.
15. Doktor, T., et al. (2011). Pore Size Distribution of Human Trabecular Bone - Comparison of Intrusion Measurements with Image Analysis. Available at: <https://www.researchgate.net/publication/258245406> (Accessed February 3, 2024).
16. Porrelli, D., et al. (2022). Trabecular bone porosity and pore size distribution in osteoporotic patients – A low field nuclear magnetic resonance and microcomputed tomography investigation. *J Mech Behav Biomed Mater*, **125**, 104926.
17. Lin, X., Patil, S., Gao, Y. G., & Qian, A. (2020). The Bone Extracellular Matrix in Bone Formation and Regeneration. *Front. Pharmacol.*, **11**, 757.
18. Zhu, L., Luo, D., & Liu, Y. (2020). Effect of the nano/microscale structure of biomaterial scaffolds on bone regeneration. *Int. J. Oral Sci.*, **12**, 36.

19. Oladapo, B. I., Zahedi, S. A., & Adeoye, A. O. M. (2019). 3D printing of bone scaffolds with hybrid biomaterials. *Compos. B Eng*, **158**, 428–436.
20. Dixon, D. T., & Gomillion, C. T. (2023). 3D-Printed conductive polymeric scaffolds with direct current electrical stimulation for enhanced bone regeneration. *J. Biomed. Mater. Res. B Appl. Biomater.*, **111**, 1351–1364.
21. Wang, Q., et al. (2021). 3D printed PCL/ β -TCP cross-scale scaffold with high-precision fiber for providing cell growth and forming bones in the pores. *Mater. Sci. Eng. C*, **127**, 112231.
22. Aunoble, S., et al. (2006). Biological performance of a new β -TCP/PLLA composite material for applications in spine surgery: In vitro and in vivo studies. *J Biomed Mater Res A*, **78**, 416–422.
23. Diez-Escudero, A., Andersson, B., Persson, C., & Hailer, N. P. (2021). Hexagonal pore geometry and the presence of hydroxyapatite enhance deposition of mineralized bone matrix on additively manufactured polylactic acid scaffolds. *Mater. Sci. Eng. C*, **125**, 112127.
24. Pereira, H. F., Cengiz, I. F., Silva, F. S., Reis, R. L., & Oliveira, J. M. (2020). Scaffolds and coatings for bone regeneration. *J. Mater. Sci. Mater. Med.*, **31**, 24.
25. Knychala, J., et al. (2013). Pore geometry regulates early stage human bone marrow cell tissue formation and organisation. *Ann. Biomed. Eng.*, **41**, 917–930.
26. Boccaccio, A., Uva, A. E., Fiorentino, M., Lamberti, L., & Monno, G. (2016). A mechanobiology-based algorithm to optimize the microstructure geometry of bone tissue scaffolds. *Int. J. Biol. Sci.*, **12**, 1–17.

27. Prochor, P., & Gryko, A. (2021). Numerical analysis of the influence of porosity and pore geometry on functionality of scaffolds designated for orthopedic regenerative medicine. *Materials*, **14**, 1–19.
28. Chen, T. H., et al. (2018). Lattice Microarchitecture for Bone Tissue Engineering from Calcium Phosphate Compared to Titanium. *Tissue Eng. Part A*, **24**, 1554–1561.
29. Van Bael, S., et al. (2012). The effect of pore geometry on the in vitro biological behavior of human periosteum-derived cells seeded on selective laser-melted Ti6Al4V bone scaffolds. *Acta Biomater.*, **8**, 2824–2834.
30. Bruyas, A., et al. (2018). Systematic characterization of 3D-printed PCL/ β -TCP scaffolds for biomedical devices and bone tissue engineering: Influence of composition and porosity. *J. Mater. Res.*, **33**, 1948–1959.
31. Backes, E. H., et al. (2021). Development and characterization of printable PLA/ β -TCP bioactive composites for bone tissue applications. *J. Appl. Polym. Sci.*, **138**, 50551.
32. Ferri, J. M., Gisbert, I., García-Sanoguera, D., Reig, M. J., & Balart, R. (2016). The effect of beta-tricalcium phosphate on mechanical and thermal performances of poly(lactic acid). *J. Compos. Mater.*, **50**, 4189–4198.
33. Karimipour-Fard, P., Jeffrey, M. P., Jones Taggart, H., Pop-Iliev, R., & Rizvi, G. (2021). Development, processing and characterization of Polycaprolactone/Nano-Hydroxyapatite/Chitin-Nano-Whisker nanocomposite filaments for additive manufacturing of bone tissue scaffolds. *J. Mech. Behav. Biomed. Mater.*, **120**, 104849.
34. Chinnasami, H., Dey, M. K., & Devireddy, R. (2023). Three-Dimensional Scaffolds for Bone Tissue Engineering. *Bioengineering*, **10**, 759.

35. Burg, K. J. L., & Shalaby, S. W. (1998). Physicochemical changes in degrading polylactide films. *J. Biomater. Sci. Polym. Ed.*, **9**, 15–29.
36. Izumiya, M., et al. (2021). Evaluation of mc3t3-e1 cell osteogenesis in different cell culture media. *Int. J. Mol. Sci.*, **22**, 1–16.
37. Schneider, M., et al. (2020). Surface etching of 3D printed poly(lactic acid) with NaOH: A systematic approach. *Polymers*, **12**, 1–20.
38. Sarkar, N., Bhumiratana, S., Geris, L., Papantoniou, I., & Grayson, W. L. (2023). Bioreactors for engineering patient-specific tissue grafts. *Nat. Rev. Bioeng.*, **1**, 361–377.
39. Zhao, F., van Rietbergen, B., Ito, K., & Hofmann, S. (2018). Flow rates in perfusion bioreactors to maximize mineralisation in bone tissue engineering in vitro. *J. Biomech.*, **79**, 232–237.
40. Papantoniou, I., et al. (2014). Spatial Optimization in Perfusion Bioreactors Improves Bone Tissue-Engineered Construct Quality Attributes. *Biotechnol. Bioeng.*, **111**, 2560–2570.

APPENDIX A: FLOWCHART

